TABLE 1. Analysis of epididymal tail weight and sperm morphology (mean ± SD) in 10-week-old wild-type and gad mice.

	Tail weight (mg)	Sperm concentration (10⁶/ml)	Defect (%)			
			Head	Midpiece	Principal piece	Detached head
wild-type	30.0 ± 0.8	23.6 ± 3.7	7.2 ± 1.5	2.4 ± 1.3	1.1 ± 0.2	2.0 ± 1.0
gad/gad	24.7 ± 1.1*	19.5 ± 3.3*	14.1 ± 2.8*	4.7 ± 1.5*	1.7 ± 0.6	3.7 ± 1.2*

* Significantly different from wild-type mice (n = 7; $P < 0.05$).

Spermatozoa Motility in gad Mice

We measured sperm motility parameters in wild-type and gad mice. Of the parameters assessed, MSP, PMP, VAP (μm/sec), VSL (μm/sec), and VCL (μm/sec) were significantly lower in gad mice. ALH (μm), linearity (%), and straightness (%) did not differ significantly between gad and wild-type mice (Fig. 7). Of the parameters we measured, the number of PMP differed most significantly between gad mice (24.4%) and wild-type mice (34.3%) (Fig. 7A).

DISCUSSION

Spermatogenesis is a highly complex process involving male germ cell proliferation and maturation from spermatogonia to spermatozoa [34]. Apoptosis is common during this process and is believed to play an important role in controlling germ cell numbers and eliminating defective germ cells that carry DNA mutations, thus ensuring the production of intact, functional spermatozoa [35–37]. Normally, germ cells are extremely sensitive to DNA damage, as such lesions are incompatible with the ultimate function of these cells [23, 24, 37]. The early apoptotic wave may result in early elimination of defective germ cells in which DNA alterations have occurred through chromosomal crossing over during the first meiotic division [23, 24, 37].

Several lines of evidence indicate that UCHL1 associates with monoubiquitin and that the monoubiquitin pool is reduced in gad mice relative to wild-type mice [18, 19, 22]. Furthermore, testes from UCHL1-deficient gad mice [22] and mice carrying the K48R mutation in ubiquitin [38] show resistance to cryptorchid-induced apoptosis, suggesting that ubiquitin is critical for modulating testicular germ cell death. Normally, damaged proteins are polyubiquitinated and degraded via the ubiquitin-proteasome system; however, if damaged proteins are not degraded as easily

when monoubiquitin is either mutated or reduced [22, 38], then germinal cells may become resistant to programmed death. Our results with the gad mouse suggest that ubiquitin induction is important for regulating programmed germinal cell death that is normally observed during the first round of spermatogenesis. We have now shown that immature testes from gad mice are resistant to the massive wave of germinal cell apoptosis during the first round of spermatogenesis. The increased resistance of UCHL1-deficient germ cells to apoptosis-inducing conditions in vivo and in vitro suggests that UCHL1 is involved in spermatogenesis (Figs. 3 and 4). The activity of the ubiquitin-proteasome system may be required for specific transitions between multiple developmental cellular processes and sequential apoptosis during spermatogenesis [6, 7, 39]. In addition, the ubiquitin-proteasome system is required for the degradation or modification of numerous germ cell-specific proteins during different phases of spermatogenesis [39–41].

Early apoptosis in testicular germ cells is regulated by a complicated signal transduction pathway. The testes contain high levels of TRP53, Bcl2 family, and caspase-3 proteins, which are targets for ubiquitination [29–31, 42–45]. However, the involvement of the ubiquitin system in the regu-
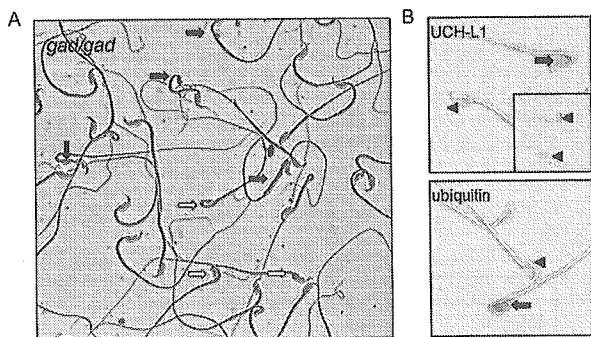

FIG. 6. A) Abnormal morphology of spermatozoa from gad mice. Spermatozoa were collected from the cauda epididymidis of 10-wk-old gad mice. Head defects (open arrows) and midpiece defects (closed arrows) are indicated. Magnification ×400. B) Immunocytochemistry of UCH-L1 and ubiquitin in wild-type and gad mice. UCHL1- and ubiquitin-positive spermatozoa (closed arrows) and normal spermatozoa (both negative, arrowheads) in wild-type mice are indicated. The inset shows an image of spermatozoa from gad mice. Magnification ×1000.
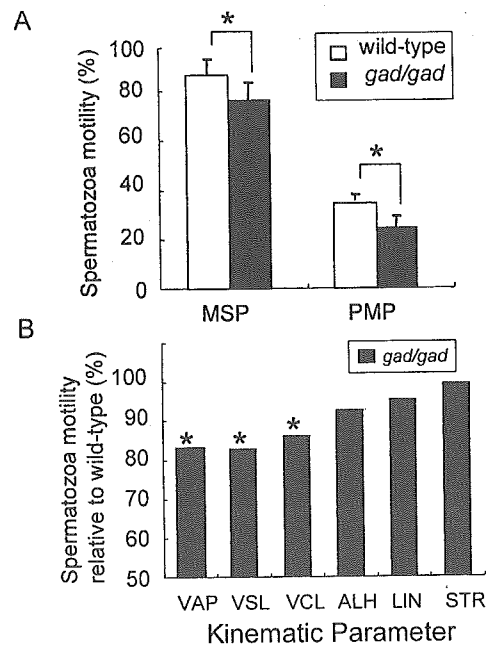

FIG. 7. Kinematic analysis of spermatozoa from the cauda epididymidis of 10-week-old wild-type and gad mice. A) Sperm motility. MSP, Percentage of motile sperm; PMP, Percentage of progressively motile sperm (n = 7; * $P < 0.05$). Data represent the mean ± SD. B) Movement characterization. VAP, Average path velocity (μm/sec); VSL, Straight-line velocity (μm/sec); VCL, Curvilinear velocity (μm/sec); ALH, Lateral head displacement (μm); LIN, Linearity (VSL/VCL × 100); STR, Straightness (VSL/VAP × 100). Data are expressed as a percentage of the values obtained for each parameter in wild-type mice (n = 7; * $P < 0.05$).

latory mechanisms of germ cell apoptosis has not been identified. A previous study showed that UCHL1-deficient *gad* mice express high levels of antiapoptotic proteins (Bcl2 family and XIAP) in the testis following cryptorchid-induced stress [22]. Alterations in the carefully maintained balance between the expression of apoptosis-inducing and apoptosis-protecting proteins may constitute one mechanism underlying the suppression of germ cell apoptosis observed in *gad* mice [46]. The decreased levels of TRP53, Bax, and caspase-3 observed in *gad* mice in this study are consistent with the suppression of germ cell apoptosis. In addition, the expression of the antiapoptotic protein Bcl-xL increased earlier in *gad* mice compared with wild-type mice. Therefore, the control of the apoptotic wave probably depends on variations in the balance between Bax and Bcl-xL [23, 47]. Analysis of the first round of spermatogenesis over time demonstrated a striking and massive wave of apoptotic germinal cells in 14-day-old mice (Fig. 3). High levels of UCHL1 protein were also observed at this age (Fig. 1) [20]. This early apoptotic wave was suppressed in the testes of *gad* mice, which had an abundance of germ cells compared with wild-type mice (Fig. 2). Moreover, the suppression of germ cell death is consistent with our previous report on cryptorchid stress injury in *gad* mice [22]. The testes of *gad* mice showed a phenotype similar to that of *Bax*-deficient mice or those overexpressing *Bcl2* or *Bcl-xL* [23, 25, 26]. Also, the testes of *Trp53*$^{-/-}$ mice exhibited a similar phenotype involving decreased germ cell apoptosis and an increased number of germ cells [48].

In the present study, we also characterized spermatozoa in *gad* mice with regard to the following reproductive endpoints: 1) the weight of reproductive organs, 2) the concentration of sperm cells, and 3) the motility and morphology of spermatozoa collected from the cauda epididymidis. The weight of cauda epididymidis from *gad* mice was significantly lower compared with that from wild-type mice. The concentration of sperm cells was also significantly lower, and most motility parameters of spermatozoa collected from the cauda epididymidis were affected in *gad* mice (Fig. 7). The significant decline in progressive forward motility, VAP, VSL, and VCL indicates that UCHL1 deficiency affects not only the ability of spermatozoa to move in the forward direction but also their vigor. In addition, the percentage of morphologically abnormal spermatozoa was significantly higher in *gad* mice (Table 1 and Fig. 6A).

Sperm production in the testis is a regulated balance between germ cell division and germ cell loss [26, 49], and there is emerging evidence that the ubiquitin-proteasome system may be central to the coordination of this process. For example, during spermatogenesis, the general activity of the ubiquitin-proteasome system is high, probably reflecting the requirement for massive degradation of cytoplasmic and nuclear proteins [6, 7, 50, 51]. Additionally, mutation of the ubiquitin-conjugating enzyme HR6B results in impaired spermatogenesis during nuclear condensation in spermatids [39, 41]. We found the fact that UCH-L1 associates with monoubiquitin in several lines of *gad* mice [18, 19, 22]. Furthermore, both proteins are expressed abundantly and at comparable levels in testis and the epididymis [11, 13, 14], suggesting that the functions of two proteins are important during spermatogenesis. Ubiquitin is present in defective spermatozoa, and proteins in these cells become ubiquitinated during epididymal passage (Fig. 6B) [11, 14, 33, 52, 53]. Furthermore, ubiquitination in the epididymis may trigger apoptotic mechanisms that recognize and eliminate abnormal spermatozoa [49, 54, 55].

Further study is required to elucidate the functional significance of the association between UCHL1 and ubiquitin during spermatozoa maturation in the epididymis. However, our observations suggest that UCHL1 may function to regulate sperm production and to ubiquitinate proteins in defective spermatozoa. Our present study demonstrates that UCHL1-deficient *gad* mice are resistant to the wave of germinal cell apoptosis that occurs during the first round of spermatogenesis and that these mice have defects in sperm production, motility, and morphology. These results suggest that UCHL1 functions in the early apoptotic wave during the first round of spermatogenesis and in the control of sperm quality during sperm maturation.

ACKNOWLEDGMENTS

REFERENCES

1. Ciechanover A, Finley D, Varshavsky A. Ubiquitin dependence of selective protein degradation demonstrated in the mammalian cell cycle mutant ts85. Cell 1984; 37:57–66.
2. Glotzer M, Murray AW, Kirschner MW. Cyclin is degraded by the ubiquitin pathway. Nature 1991; 349:132–138.
3. Strous GJ, Govers R. The ubiquitin-proteasome system and endocytosis. J Cell Sci 1999; 112(pt 10):1417–1423.
4. Wilkinson KD. Regulation of ubiquitin-dependent processes by deubiquitinating enzymes. FASEB J 1997; 11:1245–1256.
5. Hershko A, Ciechanover A. The ubiquitin system. Annu Rev Biochem 1998; 67:425–479.
6. Baarends WM, Roest HP, Grootegoed JA. The ubiquitin system in gametogenesis. Mol Cell Endocrinol 1999; 151:5–16.
7. Baarends WM, van der Laan R, Grootegoed JA. Specific aspects of the ubiquitin system in spermatogenesis. J Endocrinol Invest 2000; 23:597–604.
8. Ciechanover A. The ubiquitin-proteasome pathway: on protein death and cell life. EMBO J 1998; 17:7151–7160.
9. Weissman AM. Themes and variations on ubiquitylation. Nat Rev Mol Cell Biol 2001; 2:169–178.
10. Wing SS. Deubiquitinating enzymes—the importance of driving in reverse along the ubiquitin-proteasome pathway. Int J Biochem Cell Biol 2003; 35:590–605.
11. Fraile B, Martin R, De Miguel MP, Arenas MI, Bethencourt FR, Peinado F, Paniagua R, Santamaria L. Light and electron microscopic immunohistochemical localization of protein gene product 9.5 and ubiquitin immunoreactivities in the human epididymis and vas deferens. Biol Reprod 1996; 55:291–297.
12. Kon Y, Endoh D, Iwanaga T. Expression of protein gene product 9.5, a neuronal ubiquitin C-terminal hydrolase, and its developing change in sertoli cells of mouse testis. Mol Reprod Dev 1999; 54:333–341.
13. Kwon J, Kikuchi T, Setsuie R, Ishii Y, Kyuwa S, Yoshikawa Y. Characterization of the testis in congenitally ubiquitin carboxy-terminal hydrolase-1 (Uch-L1) defective (gad) mice. Exp Anim 2003; 52:1–9.
14. Martin R, Santamaria L, Fraile B, Paniagua R, Polak JM. Ultrastructural localization of PGP 9.5 and ubiquitin immunoreactivities in rat ductus epididymidis epithelium. Histochem J 1995; 27:431–439.
15. Pickart CM, Rose IA. Ubiquitin carboxyl-terminal hydrolase acts on ubiquitin carboxyl-terminal amides. J Biol Chem 1985; 260:7903–7910.
16. Liu Y, Fallon L, Lashuel HA, Liu Z, Lansbury PT, Jr. The UCH-L1 gene encodes two opposing enzymatic activities that affect alpha-synuclein degradation and Parkinson's disease susceptibility. Cell 2002; 111:209–218.
17. Liu Y, Lashuel HA, Choi S, Xing X, Case A, Ni J, Yeh LA, Cuny GD, Stein RL, Lansbury PT, Jr. Discovery of inhibitors that elucidate the role of UCH-L1 activity in the H1299 lung cancer cell line. Chem Biol 2003; 10:837–846.
18. Osaka H, Wang YL, Takada K, Takizawa S, Setsuie R, Li H, Sato Y, Nishikawa K, Sun YJ, Sakurai M, Harada T, Hara Y, Kimura I, Chiba S, Namikawa K, Kiyama H, Noda M, Aoki S, Wada K. Ubiquitin carboxy-terminal hydrolase L1 binds to and stabilizes monoubiquitin in neuron. Hum Mol Genet 2003; 12:1945–1958.

19. Harada T, Harada C, Wang YL, Osaka H, Amanai K, Tanaka K, Takizawa S, Setsuie R, Sakurai M, Sato Y, Noda M, Wada K. Role of ubiquitin carboxy terminal hydrolase-L1 in neural cell apoptosis induced by ischemic retinal injury in vivo. Am J Pathol 2004; 164:59–64.

20. Kwon J, Wang YL, Setsuie R, Sekiguchi S, Sakurai M, Sato Y, Lee WW, Ishii Y, Kyuwa S, Noda M, Wada K, Yoshikawa Y. Developmental regulation of ubiquitin C-terminal hydrolase isozyme expression during spermatogenesis in mice. Biol Reprod 2004; 71:515–521.

21. Saigoh K, Wang YL, Suh JG, Yamanishi T, Sakai Y, Kiyosawa H, Harada T, Ichihara N, Wakana S, Kikuchi T, Wada K. Intragenic deletion in the gene encoding ubiquitin carboxy-terminal hydrolase in gad mice. Nat Genet 1999; 23:47–51.

22. Kwon J, Wang YL, Setsuie R, Sekiguchi S, Sato Y, Sakurai M, Noda M, Aoki S, Yoshikawa Y, Wada K. Two closely related ubiquitin C-terminal hydrolase isozymes function as reciprocal modulators of germ cell apoptosis in cryptorchid testis. Am J Pathol 2004; 165:1367–1374.

23. Rodriguez I, Ody C, Araki K, Garcia I, Vassalli P. An early and massive wave of germinal cell apoptosis is required for the development of functional spermatogenesis. EMBO J 1997; 16:2262–2270.

24. Jahnukainen K, Chrysis D, Hou M, Parvinen M, Eksborg S, Soder O. Increased apoptosis occurring during the first wave of spermatogenesis is stage-specific and primarily affects midpachytene spermatocytes in the rat testis. Biol Reprod 2004; 70:290–296.

25. Furuchi T, Masuko K, Nishimune Y, Obinata M, Matsui Y. Inhibition of testicular germ cell apoptosis and differentiation in mice misexpressing Bcl-2 in spermatogonia. Development 1996; 122:1703–1709.

26. Russell LD, Chiarini-Garcia H, Korsmeyer SJ, Knudson CM. Bax-dependent spermatogonia apoptosis is required for testicular development and spermatogenesis. Biol Reprod 2002; 66:950–958.

27. Slott VL, Suarez JD, Perreault SD. Rat sperm motility analysis: methodologic considerations. Reprod Toxicol 1991; 5:449–458.

28. Goyal HO, Braden TD, Mansour M, Williams CS, Kamaleldin A, Srivastava KK. Diethylstilbestrol-treated adult rats with altered epididymal sperm numbers and sperm motility parameters, but without alterations in sperm production and sperm morphology. Biol Reprod 2001; 64:927–934.

29. Chipuk JE, Green DR. Cytoplasmic p53: Bax and forward. Cell Cycle 2004; 3:429–431.

30. Dimmeler S, Breitschopf K, Haendeler J, Zeiher AM. Dephosphorylation targets Bcl-2 for ubiquitin-dependent degradation: a link between the apoptosome and the proteasome pathway. J Exp Med 1999; 189:1815–1822.

31. Suzuki Y, Nakabayashi Y, Takahashi R. Ubiquitin-protein ligase activity of X-linked inhibitor of apoptosis protein promotes proteasomal degradation of caspase-3 and enhances its anti-apoptotic effect in Fas-induced cell death. Proc Natl Acad Sci U S A 2001; 98:8662–8667.

32. Selvakumaran M, Lin HK, Miyashita T, Wang HG, Krajewski S, Reed JC, Hoffman B, Liebermann D. Immediate early upregulation of bax expression by p53 but not TGF beta 1: a paradigm for distinct apoptotic pathways. Oncogene 1994; 9:1791–1798.

33. Sutovsky P, Moreno R, Ramalho-Santos J, Dominko T, Thompson WE, Schatten G. A putative, ubiquitin-dependent mechanism for the recognition and elimination of defective spermatozoa in the mammalian epididymis. J Cell Sci 2001; 114:1665–1675.

34. de Kretser DM, Loveland KL, Meinhardt A, Simorangkir D, Wreford N. Spermatogenesis. Hum Reprod 1998; 13(suppl 1):1–8.

35. Gosden R, Spears N. Programmed cell death in the reproductive system. Br Med Bull 1997; 53:644–661.

36. Matsui Y. Regulation of germ cell death in mammalian gonads. APMIS 1998; 106:142–147Ascussion 147–148.

37. Print CG, Loveland KL. Germ cell suicide: new insights into apoptosis during spermatogenesis. Bioessays 2000; 22:423–430.

38. Rasoulpour RJ, Schoenfeld HA, Gray DA, Boekelheide K. Expression of a K48R mutant ubiquitin protects mouse testis from cryptorchid injury and aging. Am J Pathol 2003; 163:2595–2603.

39. Baarends WM, Wassenaar E, Hoogerbrugge JW, van Cappellen G, Roest HP, Vreeburg J, Ooms M, Hoeijmakers JH, Grootegoed JA. Loss of HR6B ubiquitin-conjugating activity results in damaged synaptonemal complex structure and increased crossing-over frequency during the male meiotic prophase. Mol Cell Biol 2003; 23:1151–1162.

40. Baarends WM, Hoogerbrugge JW, Roest HP, Ooms M, Vreeburg J, Hoeijmakers JH, Grootegoed JA. Histone ubiquitination and chromatin remodeling in mouse spermatogenesis. Dev Biol 1999; 207:322–333.

41. Roest HP, van Klaveren J, de Wit J, van Gurp CG, Koken MH, Vermey M, van Roijen JH, Hoogerbrugge JW, Vreeburg JT, Baarends WM, Bootsma D, Grootegoed JA, Hoeijmakers JH. Inactivation of the HR6B ubiquitin-conjugating DNA repair enzyme in mice causes male sterility associated with chromatin modification. Cell 1996; 86:799–810.

42. Marshansky V, Wang X, Bertrand R, Luo H, Duguid W, Chinnadurai G, Kanaan N, Vu MD, Wu J. Proteasomes modulate balance among proapoptotic and antiapoptotic Bcl-2 family members and compromise functioning of the electron transport chain in leukemic cells. J Immunol 2001; 166:3130–3142.

43. Oren M. Regulation of the p53 tumor suppressor protein. J Biol Chem 1999; 274:36031–36034.

44. Orlowski RZ. The role of the ubiquitin-proteasome pathway in apoptosis. Cell Death Differ 1999; 6:303–313.

45. Yang Y, Yu X. Regulation of apoptosis: the ubiquitous way. FASEB J 2003; 17:790–799.

46. Beumer TL, Roepers-Gajadien HL, Gademan IS, Lock TM, Kal HB, De Rooij DG. Apoptosis regulation in the testis: involvement of Bcl-2 family members. Mol Reprod Dev 2000; 56:353–359.

47. Borner C. The Bcl-2 protein family: sensors and checkpoints for life-or-death decisions. Mol Immunol 2003; 39:615–647.

48. Yin Y, Stahl BC, DeWolf WC. Morgentaler A. p53-mediated germ cell quality control in spermatogenesis. Dev Biol 1998; 204:165–171.

49. Sutovsky P. Ubiquitin-dependent proteolysis in mammalian spermatogenesis, fertilization, and sperm quality control: killing three birds with one stone. Microsc Res Tech 2003; 61:88–102.

50. Rajapurohitam V, Bedard N, Wing SS. Control of ubiquitination of proteins in rat tissues by ubiquitin conjugating enzymes and isopeptidases. Am J Physiol Endocrinol Metab 2002; 282:E739–E745.

51. Rajapurohitam V, Morales CR, El-Alfy M, Lefrancois S, Bedard N, Wing SS. Activation of a UBC4-dependent pathway of ubiquitin conjugation during postnatal development of the rat testis. Dev Biol 1999; 212:217–228.

52. Lippert TH, Seeger H, Schieferstein G, Voelter W. Immunoreactive ubiquitin in human seminal plasma. J Androl 1993; 14:130–131.

53. Sutovsky P, Terada Y, Schatten G. Ubiquitin-based sperm assay for the diagnosis of male factor infertility. Hum Reprod 2001; 16:250–258.

54. Sinha Hikim AP, Swerdloff RS. Hormonal and genetic control of germ cell apoptosis in the testis. Rev Reprod 1999; 4:38–47.

55. Sutovsky P, Hauser R, Sutovsky M. Increased levels of sperm ubiquitin correlate with semen quality in men from an andrology laboratory clinic population. Hum Reprod 2004; 19:628–638.

ELSEVIER

Clinico-pathological rescue of a model mouse of Huntington's disease by siRNA

Yu-Lai Wang [a,b,1], Wanzhao Liu [a,b,1], Etsuko Wada [a], Miho Murata [a,b],
Keiji Wada [a,b], Ichiro Kanazawa [a,b,*]

[a] *Department of Degenerative Neurological Diseases, National Institute of Neuroscience, National Center of Neurology and Psychiatry (NCNP), Tokyo 187-8502, Japan*
[b] *Solution Oriented Research for Science and Technology (SORST), Japan Science and Technology Agency (JST), Saitama 332-0012, Japan*

Abstract

Huntington's disease (HD) is an autosomal dominant inheritable neurodegenerative disorder currently without effective treatment. It is caused by an expanded polyglutamine (poly Q) tract in the corresponding protein, huntingtin (htt), and therefore suppressing the huntingtin expression in brain neurons is expected to delay the onset and mitigate the severity of the disease. Here, we have used small interfering RNAs (siRNAs) directed against the huntingtin gene to repress the transgenic mutant huntingtin expression in an HD mouse model, R6/2. Results showed that intraventricular injection of siRNAs at an early postnatal period inhibited transgenic huntingtin expression in brain neurons and induced a decrease in the numbers and sizes of intranuclear inclusions in striatal neurons. Treatments using this siRNA significantly prolonged model mice longevity, improved motor function and slowed down the loss of body weight. This work suggests that siRNA-based therapy is promising as a future treatment for HD.
© 2005 Elsevier Ireland Ltd and the Japan Neuroscience Society. All rights reserved.

1. Introduction

Huntington's disease (HD) is a choreic-psychiatric neurodegenerative disease that is inherited in an autosomal dominant manner. HD is caused by an expansion of CAG repeats (more than 35) in the HD gene, yielding an expanded polyglutamine (poly Q) tract in the protein, huntingtin (htt) (Gusella and MacDonald, 2000). Pathologically, HD is characterized by selective loss of brain neurons and the formation of intranuclear aggregates (inclusion bodies) composed of htt and other functional proteins in the remaining neurons (Hazeki et al., 2002; Busch et al., 2003). Transgenic mice with human htt exon 1 containing expanded CAG repeats displayed abnormal behavior as well as

ubiquitinated neuronal intranuclear inclusions (NIIs) composed of poly Q aggregations found in the striatal and cortical neurons, revealing that mutant htt exon 1 is sufficient to cause the disease (Mangiarini et al., 1996). There is, however, a controversy as to whether NIIs are harmful to living cells or act in their defense by sequestering toxic soluble mutant htt (Kaytor et al., 2004). In this regard, there is a general consensus that cytosolic mutant htt forms invisible or minute aggregates that adversely affect cell survival (Trushina et al., 2003) through dysregulation or upregulation of CRE-mediated transcription (Gines et al., 2003; Obrietan and Hoyt, 2004; Sugars et al., 2004). All of these findings suggest that the expression of the mutant huntingtin may cause the disease via a "gain-of-function" mechanism. Down-regulation of mutant huntingtin expression has been suggested to be a promising therapeutic strategy (Haque et al., 1997). Yamamoto et al. (2000), using a conditional mouse model of HD,

* Corresponding author. Tel.: +81 42 3461780; fax: +81 42 3461762.
  E-mail address: ichiro@ncnp.go.jp (I. Kanazawa).
[1] Both these authors contributed equally to this work.

demonstrated that "switching off" the transgenic htt expression at the adult age would lessen the severity of the disease, suggesting that HD might be reversible. Thus, we expected that suppression of mutant htt gene expression in brain neurons would constitute a reasonable clinical approach to combat HD.

Several techniques have been explored to block the expression of huntingtin expression, including antisense technology (Boado et al., 2000; Nellemann et al., 2000) and catalytic DNA (Yen et al., 1999). Small interfering RNAs (siRNAs) offer a much more powerful means to selectively silence genes by base-pairing in mammalian somatic cells, and these RNAs are very specific, stable and highly efficient. Recently, we have identified highly effective and specific siRNAs against huntingtin exon 1 mRNA using cell culture models (Liu et al., 2003). Here, we delivered these siRNAs into brain neurons of newborn HD transgenic mice (R6/2) to test whether the model mice can benefit from siRNA treatment.

2. Materials and methods

2.1. HD model mouse

HD transgenic mice (R6/2) were purchased from Jackson Laboratory (Bar Harbor, Maine). The strain was maintained by crossing ovarian transplant hemizygote females with wild-type B6CBAF1/J males following the protocol of Jackson Laboratory. The HD transgene comprises about 1 kb of the human HD gene and includes the promoter, 5' untranslated region (5' UTR), and exon 1 with 144 CAG repeats (Mangiarini et al., 1996). Offsprings were genotyped by PCR using tail tip total genomic DNA following the protocol of Jackson Laboratory. Because the highly expanded CAG repeats are unstable in transgenic mice, especially on paternal transmission (Mangiarini et al., 1997), we used only F1 generation in this work. All the mutant htt transgenic mice (half in F1 generation) used here have a transgenic mutant htt allele with same or nearly same CAG repeat number. The wild-type littermates, B6CBAF1/J, were used as controls. The mice were housed one to five per cage with food and water available. Animal care and handling were in accordance with institutional regulations for animal care and were approved by the Animal Investigation Committee of the National Institute of Neuroscience, NCNP, Japan.

2.2. siRNAs

Single-stranded 21-nt RNAs (siRNA-HDExon1, sense strand, 5'-GCCUUCGAGUCCCUCAAGUCC-3'; antisense strand, 3'-UCCGGAAGCUCAGGGAGUUCA-5') were custom synthesized and HPLC-purified (Qiagen, Huntsville, AL) and annealed as described previously (Liu et al., 2003). A non-silencing siRNA was used as control (Qiagen).

2.3. Cell culture and transfection

Cell lines and the recombinant htt72Q-d1EGFP fusion protein expression vectors were as previously described (Liu et al., 2003). Protocols for cell culture and co-transfection using Lipofectamine 2000 (Invitrogen, Carlsbad, CA) of siRNAs and htt72Q-d1EGFP vectors were same as described previously (Liu et al., 2003). Cos-7, SH-SY5Y and Neuro-2A cell lines were used. Cells were grown in Minimum Essential Medium-Alpha Medium (Gibco BRL) (for Cos-7), or in Dulbecco's Modified Eagle's Medium (Gibco BRL) (for SH-SY5Y and Neuro-2A) supplemented with 10% heat-inactivated fetal bovine serum (FBS, Mitsubishi Kasei) and antibiotics (10 units/ml of penicillin and 50 μg/ml of streptomycin; Meiji). A 12-well plate was used to perform co-transfection experiments of httQ72-d1EGFP and siRNAs. Forty eight hours after co-transfection, cultured plates were observed under fluorescence microscopy to examine the expression level and the distribution of fused huntingtin-EGFP proteins.

2.4. In vivo transfection

To test the silencing effects of siRNAs, we cotransfected httQ72-d1EGFP and siRNAs into new-born mouse (wild-type, P2) brain neurons using ExGen 500 that is designed for in vivo transfection. We followed the manufacturer's protocols and adjusted the ExGen 500/(vectors + siRNAs) ratio (N/P ratio) to 6, and injected 5 μl of the solution containing 0.25 μg of httQ72-d1EGFP and 0.2 μg of siRNAs. Mice were sacrificed 96 h after transfection, and brain tissues were taken out and sectioned to examine under fluorescence microscopy.

To evaluate their efficiency of siRNAs delivery and cytotoxicity in vivo, two commercially available transfection reagents, Lipofectamine 2000 (Invitrogen) and ExGen 500 (Fermentas, Hanover, MD) were tested in wild-type mice. In experiments using ExGen 500, we followed the manufacturer's protocols and adjusted the ExGen 500/siRNA ratio (N/P ratio) to 6, and 5 μl of transfection solution was applied for each mouse. When using Lipofectamine 2000, each mouse received about 5 μl of transfection complex solution containing 0.2 μg siRNAs and 0.5 μl Lipofectamine 2000. A 10 μl microsyringe was used to inject the transfection complex solution. The delivery efficiency of ExGen 500 is very high but it seems it is also more toxic compared to Lipofectamine 2000 (data not shown). The cytotoxicity caused by Lipofectamine reagent seems very minor in P2 mice brain, but perhaps its delivery efficiency is lower than ExGen 500. Finally, we chose the Lipofectamine 2000 reagent to deliver siRNA. The three experimental controls: buffer-treated, control siRNA-treated and untreated were used. For each newborn (P2) mouse, transfection solution was directly injected into lateral ventricle to a depth of 2.0 mm approximately at the position of 1 mm to the right of and 1 mm posterior from Bregma, as

previously reported (Shen et al., 2001, 2002; Sakurai et al., 2004). Since there is no suitable method to directly detect the siRNA for histology, 5 μl of Alcian blue dye was injected into normal mice at P2 in order to define the site of injection of the siRNA via histological examination of brain sections. The immediate analysis revealed that in most cases the dye was injected into the lateral ventricle (data not shown). P2 mouse injections were typically made blindly with respect to genotype. About 4 weeks after injection, all genotyping was performed by PCR using genomic DNA from tail biopsies.

2.5. Quantitative RT-PCR

Two to 14 days after injecting the siRNA/transfection complexes, the mice were sacrificed and whole brain tissues were collected ($n = 3$ for each group). Transgenic mRNA was estimated by quantitative RT-PCR using SYBR Green PCR master mix on an ABI 7700 sequence detector. Primers were: forward, 5′-CGCCGCCTCCTCAGCTTCCT-3′ and reverse, 5′-GCGGTGGTGGCGGCGGCGGCT-3′. Expression of GAPDH and β-actin were also estimated in each sample using the same methods as controls.

2.6. Western blot analysis

Protein lysates from the striatum were extracted using NE-PER Nuclear and Cytoplasmic Extraction Reagents (Pierce). Approximately 50 μg of nuclear protein extracts were loaded per lane on 5–10% gradient SDS-PAGE gels. The proteins were electrophoretically transferred to Immobilon-P membranes (0.45 μm, Millipore, Bedford, MA). Primary antibodies were directed against huntingtin (MAB5374, Chemicon, Temecula, CA). Anti-β-actin antibody (Sigma) was used as an internal control. Immunoreactions were visualized using the SuperSignal West Dura Extended Duration Substrate (Pierce, Rockford, IL) and analyzed with a ChemiImager (Alpha Innotech, CA).

2.7. Immunohistochemistry

Brains from mice ($n = 3$ for each group) were fixed in 4% paraformaldehyde (PFA) in phosphate-buffered saline (PBS, pH 7.4) and embedded in paraffin. Sections (4-μm) were used for immunohistochemistry by mouse monoclonal anti-huntingtin antibody (MAB5374, 1:500). Subsequent antibody detection was carried out using anti-mouse IgG from the Vectorstain Elite ABC kit (Vector Labs, Burlingame, CA).

2.8. Assessment of symptoms

2.8.1. Body weight

Body weight was measured weekly for all surviving mice from ages 4 to 17 weeks, including wild-type or transgenic, treated or untreated.

2.8.2. Tail suspension test

Mice over 4 weeks old were suspended by their tails for 15 s, during which the limbs of R6/2 may exhibit a feet-clasping posture not observed in wild-type mice. Mice showing feet-clasping posture during the 15 s suspension were scored positive.

2.8.3. Rotarod test

Forced motor activity was tested with an accelerating rotarod (Ohara, Japan). The mice were placed on the inactive drum and then forced to walk in the forward direction as the drum was accelerated from 3 to 30 rpm over a period of 300 s. The time until the animal fell off the drum was noted, with a cutoff of 300 s. Mice (siRNA-treated: $n = 17$, mock-treated: $n = 10$, untreated: $n = 11$) were tested at 6, 7 and 8 weeks of age. At each time point, the mice were tested on 2 consecutive days, for three trials per day. Data used in statistical analyses were from the second day, since the first day was for the mice to learn the task.

2.8.4. Open-field analysis

The pattern of movement of each mouse was monitored for 10 min in a 50 cm × 50 cm open field chamber (Ohara, Japan) made of gray polyvinyl chloride. The floor of the open field was divided into 25 equal quadrants by 5 cm × 5 cm perpendicular black lines. A video camera was mounted 80 cm above the field and connected to a Macintosh G4 computer. Diffuse white light provided an illumination density of approximately 0.4 lx at the center of the field. The mice were given three training sessions to acclimatize them to the open-field equipment. The mice were placed into the foremost right corner and observed for 10 min. Data for movement trace, distance and positions at a corresponding time were recorded by the computer and analyzed using Image OF 2.03, a modified software program based on the public domain NIH Image program (developed at the U.S. National Institutes of Health and available on the Internet at http://rsb.info.nih.gov/nih-image/). After each trial, the apparatus was cleaned with 70% alcohol.

2.8.5. Survival analysis

The dates of birth and death were recorded for every R6/2 mouse to calculate longevity (days) for each mouse and for a further survival analysis.

3. Results

3.1. Effects of siRNAs on htt expression in vitro and in vivo

We designed a 21-nucleotide siRNA (siRNA-HDExon1, Fig. 1(B)) targeted against the sequence (underlined in red) at immediate upstream of the CAG repeats of human htt (Fig. 1(A), underlined in green). Cultured Cos-7 cells cotransfected with httQ72-d1EGFP and siRNA-HDExon1
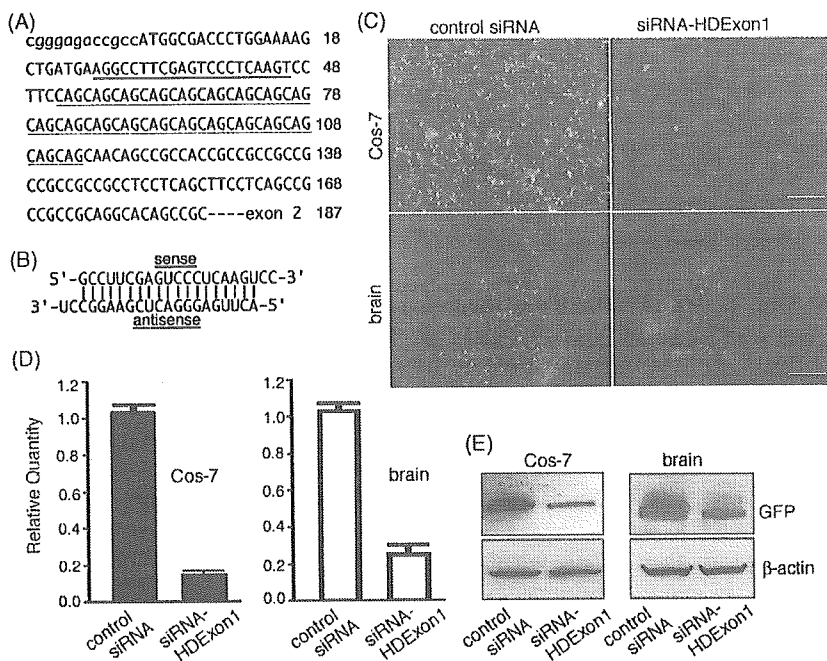
Fig. 1. siRNA-HDExon1 is effective and specific in vivo and in vitro. (A) cDNA sequence showing the target position for siRNA-HDExon1 (red underline) and CAG repeats (green underline) in the first exon of the human huntingtin gene. (B) Sequences and predicted structure for the siRNA-HDExon1. (C) Representative images showing the effects of siRNA-HDExon1 against the httQ72-d1EGFP fusion protein in Cos-7 cells (upper panels) and newborn mouse brain neurons (lower panels), respectively. Scale bar, 200 μm. (D) Quantitative RT-PCR results showing the knock-down of targeted httQ72-d1EGFP mRNA by siRNA-HDExon1 in vitro using cultured Cos-7 cells (left panel), and in vivo by transfection of newborn mouse brain (right panel). (E) Western blots showing down-regulation of the targeted httQ72-d1EGFP fusion protein in Cos-7 cell lysates and brain lysates. β-actin was used as a protein loading control.
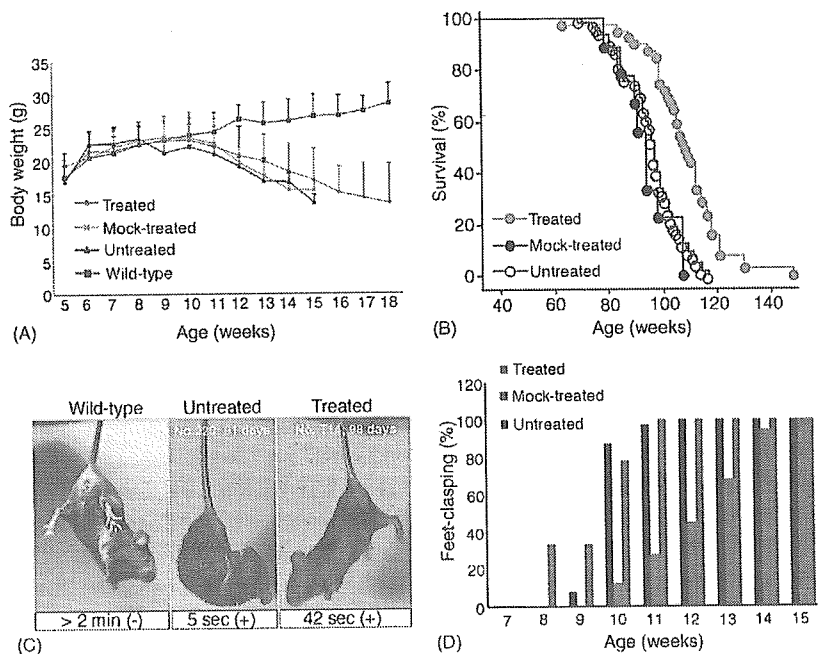

Fig. 2. Effects of siRNA-HDExon1 on the symptomatic phenotypes of the HD mouse model. (A) Effect of siRNA-HDExon1 on body weight in R6/2 mice. Body weight loss was delayed in the siRNA-HDExon1-treated group compared with the mock-treated or untreated groups (statistically significant at 13, 14 and 15 weeks; $p < 0.01$ by ANOVA). Vertical bars indicate S.D. (B) Survival curves (Kaplan–Meier method) showing that siRNA-HDExon1 treatment extended the longevity of R6/2 mice significantly ($p < 0.0001$ by log-rank test; siRNA-treated, $n = 39$; mock-treated, $n = 9$; untreated, $n = 65$). Wild-type mice that had the same treatment had a normal lifespan. (C) Representative images showing the effect of siRNA-HDExon1 on the test for the feet-clasping phenotype during tail suspension. A 13-week-old untreated R6/2 mouse displayed the feet-clasping posture at 5 s (center), whereas a 14-week-old R6/2 mouse treated with siRNA-HDExon1 did not display it until 42 s (right). (D) The treatment of siRNA-HDExon1 significantly delayed the age of feet-clasping (siRNA-treated, $n = 41$; mock-treated, $n = 12$; untreated, $n = 48$). The y-axis of the graph shows the percentage of mice that displayed the feet-clasping posture during the 15 s test period.

showed that the siRNAs efficiently suppressed the expression of recombinant httQ72-d1EGFP, while the control siRNAs (Qiagen, non-silencing control siRNAs) did not affect the expression (Fig. 1(C) upper panels). The suppression was confirmed by quantitative RT-PCR and Western blot analysis. As shown in Fig. 1(D) (left), cells transfected with the siRNA-HDExon1 reduced the expression of cognate htt-EGFP mRNA. Western blots showed a lowered htt-EGFP protein level in siRNA-HDExon1-treated cells (Fig. 1(E), left). Similar results were obtained in experiments using cultured SH-SY5Y and Neuro-2A cells, revealing that the suppressive effects did not differ significantly among cell types (data not shown). Besides, the siRNA-HDExon1 efficiently down-regulated the endogenous htt expression in cultured human cells (Liu et al., 2003).

Since chemically synthesized siRNAs were effective and specific in cell culture models, we then tested whether siRNA-HDExon1 was effective in mouse brain neurons through in vivo cotransfection with httQ72-d1EGFP constructs. Fig. 1(C) (lower panels) showed that siRNA-HDExon1 effectively knocked down the httQ72-d1EGFP expression in newborn mouse brain neurons (Fig. 1(C), lower panels). These effects were also confirmed by quantitative RT-PCR (Fig. 1(D), right), and by Western blots (Fig. 1(E), right). Both htt-EGFP mRNA and protein were suppressed in the mouse treated with siRNA-HDExon1 compared with those treated by a non-silencing control siRNA (Qiagen).

These results indicate that siRNA-HDExon1 is highly effective in HD gene suppression both in vitro and in vivo. We next applied this siRNA to the HD model mouse, R6/2 to test if it is beneficial.

3.2. Effects of siRNAs on HD transgenic model mice, R6/2

3.2.1. Change of body weight

The growth of R6/2 mice was normal before the onset of the HD-like phenotypes caused by transgenic mutant htt exon 1 containing expanded CAG repeats (Mangiarini et al., 1996). From ages 8 to 9 weeks, due to the expression of the transgenic HD exon 1 and subsequent accumulation of mutant htt, R6/2 mice had an obviously smaller body size compared with age-matched wild-type mice. Deaths occurred at 14–15 weeks of age with a significant loss of body weight. We analyzed the body weight change in line with ages (weeks) among siRNA-treated group ($n = 27$), untreated group ($n = 22$), control siRNA-treated group ($n = 4$), and buffer-treated group ($n = 8$). Since there was no significant difference in the results between the control siRNA-treated group and the buffer-treated group, we pooled the data together as a "mock-treated" group ($n = 12$). The results showed that the progressive body-weight loss of HD mice treated by siRNA-HDExon1 was slowed down compared with untreated and mock-treated

groups (Fig. 2(A)). Mock-treated and untreated R6/2 transgenic mice start to lose body weight aggressively from around 8 to 9 weeks of age, while the loss was less severe in siRNA-HDExon1-treated R6/2 mice ($p < 0.01$ by ANOVA).

3.2.2. Longevity

The average longevity of HD mice received siRNA-HDExon1 treatment is 109.2 ± 12.3 (mean $\pm$ S.D., in days, $n = 39$), while it is 93.9 ± 9.2 days for mock-treated group ($n = 9$) and 95.7 ± 10.5 days for untreated group ($n = 65$). A comparative survival analysis (Kaplan–Meier method) clearly indicated that lifespan of siRNA-HDExon1-treated HD mice extended by more than 2 weeks (Fig. 2(B)). The effect was statistically significant ($p < 0.0001$ by log-rank test). Furthermore, among the 39 siRNA-treated R6/2 mice, three survived longer than 133 days, and one of these lived to 147 days (21 weeks). Therefore, treatment of siRNA-HDExon1 apparently slowed onset of HD-like phenotype and extended the life span of R6/2 mice.

3.2.3. Motor function

We assessed the effects of siRNA-HDExon1 on the motor function before and after HD-like symptoms onset. We first examined the feet-clasping phenotype which is commonly accepted as an indicator of HD-like disease onset in various HD mouse models (Menalled and Chesselet, 2002). Treatment with this siRNA clearly delayed the onset and reduced the frequency of the feet-clasping behavior triggered by tail suspension, which usually manifests at ∼8 weeks of age for untreated R6/2 mice (Fig. 2(C and D), siRNA-treated, $n = 41$; mock-treated, $n = 12$; untreated, $n = 48$). This implied that siRNA treatments delayed the age of onset of HD symptoms by interfering with the expression of the transgenic mutant htt.

Rotarod tests were performed on R6/2 mice weekly at 6–8 weeks of age. siRNA-HDExon1-treated R6/2 mice ($n = 17$) performed significantly better than untreated R6/2 mice ($n = 11$; $p < 0.05$ by t-test; Fig. 3(A)) and were comparable to wild-type controls, thus indicating a beneficial effect of siRNA-treatment even at this stage. We also examined the pattern of free movement of mice at 9, 12 and 14 weeks of age using open-field equipment (Fig. 3(B)). siRNA-HDExon1-treated mice were more active than untreated or mock-treated R6/2 mice, especially at ages over 12 weeks. These data again suggest that siRNA-HDExon1 treatment can delay disease progression by about 2 weeks.

3.3. Pathological examinations

The formation of the intranuclear aggregation of mutant htt have been identified in human HD patients, and are accepted as pathological indicators of neuronal degeneration caused by mutated htt (DiFiglia et al., 1997). This NII formation is also a common phenomenon in both cell culture
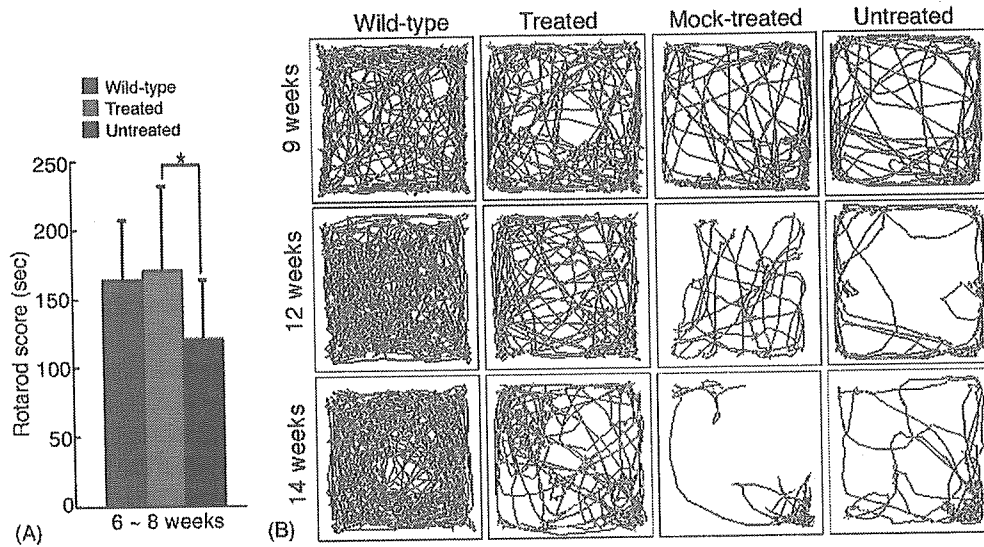
Fig. 3. Motor function assessment using a rotarod and open-field equipment. (A) R6/2 mice treated with siRNA-HDExon1 showed significant improvement on the rotarod at 6–8 weeks of age (*t*-test, $^*p < 0.05$; siRNA-treated, $n = 17$; mock-treated, $n = 10$; untreated, $n = 11$). (B) Open-field test. Trace comparison for age-matched groups of wild-type, siRNA-HDExon1-treated, mock-treated, or untreated R6/2 mice. siRNA-HDExon1-treated mice were more active than untreated or mock-treated R6/2 mice, especially at ages over 12 weeks.

models and in model animals. In HD transgenic mice, NII formation is commonly accepted as a pathological hallmark (Menalled and Chesselet, 2002). Because the transcription level relates to protein expression, the relative amounts of htt mRNA were estimated by real-time PCR to investigate the duration of the effect of siRNA on htt mRNA levels. The results showed that the suppression of htt mRNA was maintained for more than 1 week (Fig. 4(A)). The amount of htt aggregates in the striatum, as estimated by Western blotting, was reduced in the nuclear fraction of siRNA-treated mice (Fig. 4(B)). The soluble htt was not detected as previously reported (Tanaka et al., 2004). Therefore, siRNAs against transgenic htt induced the degradation of htt mRNA, which in turn resulted in a reduction of intranuclear

aggregations on mutant htt. This confirms that siRNA treatment is pathologically beneficial.

The ventricles of untreated R6/2 mice (>8 weeks of age) were larger than those of wild-type mice, due largely to general brain atrophy and compensation by the ventricular system. SiRNA-HDExon1 treatment lessened the severity of this defect (Fig. 5(A)). As mentioned above, the occurrence of NII in brain neurons are widely accepted as pathological indicators of neuronal degeneration caused by mutated htt containing a poly Q in the R6/2 mouse model. In our experiments, immunohistochemical analysis of mouse brains using an antibody against htt clearly demonstrated that siRNA treatment reduced the prevalence of aggregates in the striatum compared with untreated or mock-treated R6/
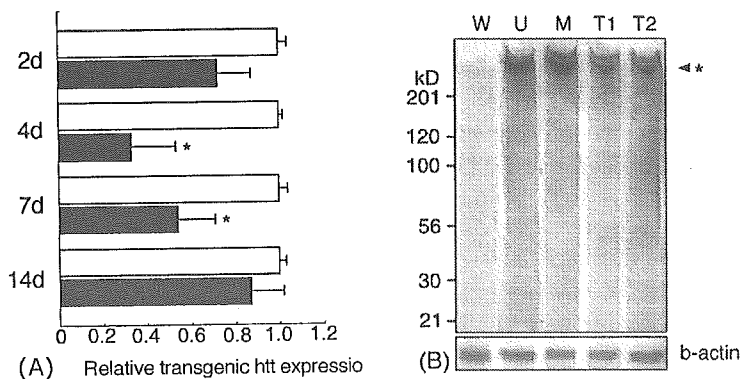

Fig. 4. siRNA-HDExon1 significantly reduces huntingtin transgenic mRNA and protein levels in brain tissues of R6/2 mice. (A) RNA from whole brain extracts was isolated, and huntingtin transgenic mRNA was determined by real-time PCR. siRNA-HDExon1-treated mice (black bars) suppressed transgene mRNA compared with the control group (combined mock-treated and untreated mice, white bars). Transgene expression was maximally repressed at 4 days post-transfection in vivo, and its effects lasted for at least 7 days ($n = 3$ for each group, $^*p < 0.01$). (B) Western blots of huntingtin aggregates in striatal tissue (50 μg per lane, nuclear extracts) from each group at 8 weeks of age. W, wild-type; U, untreated; M, mock-treated; T1, siRNA-treated mouse #1; T2, siRNA-treated mouse #2. Aggregated proteins remained in the gradient gel, as indicated (*, >200 kDa).
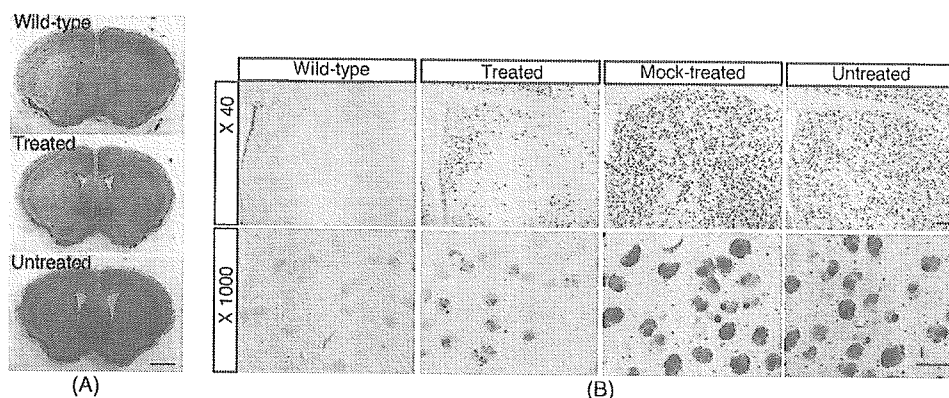
Fig. 5. Brain atrophy was inhibited and huntingtin-immunoreactive intranuclear inclusions were significantly reduced in siRNA-HDExon1-treated R6/2 mice. (A) Effect of siRNA-HDExon1 on ventricular enlargement and striatal atrophy. Upper panel, wild-type; middle panel, siRNA-treated; lower panel, untreated. Scale bar: 100 μm. (B) Brains from 8-week-old mice were immunostained with an antibody against mutant huntingtin (MAB5374), which recognizes the N-terminal portion of this protein. Neuronal intranuclear inclusions of mutant huntingtin were abundant in the striatum of mock-treated and untreated R6/2 mice. Compared with those mice, siRNA-HDExon1-treated R6/2 mice showed a decrease in number of cells with intranuclear inclusions in the striatum. Scale bars: 200 μm for upper panels (magnification ×40) and 30 μm for lower panels (magnification ×1000).

2 mice of the same age (8 weeks; Fig. 5(B)). However, these effects were locally confirmed in the striatum especially at the injection site, but not in remote areas of the ventricle such as the cortex. We also noticed that, in siRNA-treated mice, NII-positive neurons were not evenly distributed in different areas of the striatum, perhaps a consequence of the uneven diffusion of the solution containing the siRNA-transfection complex following the initial injection into the brain (Fig. 5(B)).

4. Discussion

Using cultured cells or HD model mice, there are numerous experimental approaches to address potential therapeutic strategies for HD based on different principles (Chen et al., 2000; Ferrante et al., 2003; Tanaka et al., 2004). However, since the expression of mutant htt in neurons is a crucial and fundamental event in HD in terms of "gain-of-function" theory (Kennedy et al., 2003; Schaffar et al., 2004), the most plausible strategy to combat HD would be to suppress mutant htt expression specifically in the brain. HD transgenic mice, R6/2, develop a neurodegenerative syndrome that closely models the human disease. Here we show that siRNA treatment of these mice from an early age helps to prevent the loss of body weight, extend longevity and delay the onset of motor dysfunction. Besides these beneficial effects, siRNAs induce down-regulation of transgenic htt expression and decrease the density and number of NII in striatal neurons. This work may represent the first successful use of siRNA in HD mouse model R6/2.

Surprisingly, a beneficial effect of siRNA could be attained after only one intraventricular injection, just after birth. Moreover, the effect was unexpectedly long lasting. The silencing effect of siRNA in replicating cells usually reaches a maximum around the fourth day and lasts no longer than 1 week (Novina et al., 2002; Tuschl, 2002). Although there is little evidence for the long-lasting effect of siRNA in post-mitotic cells such as neurons or muscle cells, the effect of siRNA has been sustained for at least 15 days in non-dividing macrophages (Song et al., 2003). It is, therefore, quite striking that the effect of the siRNA, siRNA-HDExon1, was apparently sustained so as to prolong the lifespan of R6/2 (Fig. 2(B)). The sustained siRNA effect in the brain could have been due to a reduced degradation rate of siRNA in post-mitotic cells via an unknown mechanism. However, another possibility is that the single application of siRNA-HDExon1 could have had a long-lasting suppressive effect on protein synthesis.

One of the distinct characteristics of HD is that its development is progressive, with onset occurring in middle age in human patients. Now that a pre-symptomatic genetic test is available, pre-clinical treatment may be feasible. An important point is the age at which a pre-symptomatic HD patient should begin preclinical treatment. Our work now shows that the application of siRNA directly into the brain of newborn mice (P2) results in significant improvement in both the symptoms and motor function of these HD model animals. We therefore postulate that the use of siRNA soon after birth—before NII formation/accumulation begins—may suppress mutant htt expression and thus block disease development.

Even though our results are very encouraging, there are still many experimental details to be investigated prior to the use of this technology in the clinic. We must refine our ability to efficiently and stably produce and deliver sufficient amounts of siRNA to the proper target tissues. Researchers have recently used plasmid and viral vectors to transcribe short-hairpin RNAs (shRNA), both in vitro and in vivo. Viral vectors expressing an shRNA directed against the mutant *SCA1* gene functioned similarly to

siRNA to rescue the clinical symptoms and pathology of a mouse model of spinocerebellar ataxia 1, another disease related to expanded CAG repeats (Xia et al., 2004). During the editorial process of this paper, Harper et al. (2005) have shown that RNA interference induced by viral vectors improves motor and neuropathological abnormalities in another HD mouse model which is HD transgenic containing 82 CAG repeats and with a milder HD-like phenotype compared to R6/2 used here (Harper et al., 2005). Although vector-based shRNA-mediated RNAi activates interferon response in vitro, whereas siRNA does not induce the type 1 interferon response (Bridge et al., 2003), this system achieves more stable inhibition of gene expression compared with transient delivery of chemically synthesized siRNA. We have also generated such vectors against the htt gene and proved them to be effective and specific in cell culture models. Their effects on R6/2 are now being tested.

Compared with adenoviral vectors (10^{10} pfu/ml), gene expression following cationic DNA-liposome complex transfection is approximately 20-fold lower, but without biochemical, hematological and histopathological abnormalities (Stephan et al., 1996). Thus, we conclude that a delivery system with little or no toxicity, but with high efficiency and selectivity, is required before clinical trials. Although there were some minor variations among individual mice, the distribution pattern of the dye injected with the DNA-liposome complex was consistent and reproducible, and our results do not reflect non-specific technical aspects of the injection procedure.

Wild-type htt is essential for embryogenesis since an htt gene knockout in mice causes early embryonic lethality (Duyao et al., 1995; Nasir et al., 1995; Zeitlin et al., 1995). Conditional knockout of the mouse htt gene after postnatal day 5 results in progressive neurodegeneration in the adult mouse (Dragatsis et al., 2000). It would therefore be ideal to reduce the expression of the mutant htt gene independently of the wild-type gene. However, it has been practically impossible to design an siRNA sequence that is selective for mutant htt. In this study, there are three base pair differences in the siRNA-HDExon1 targeted region of mouse htt, and siRNA may not suppress mouse homologous huntingtin expression. We currently have no data on whether siRNA-HDExon1 reduced expression of mouse endogenous htt in vivo, except that we did not identify any affected phenotypes in siRNA-treated wild-type mouse.

We have shown that siRNA can improve the clinical and pathological abnormalities manifested by an animal model of HD. We obtained our results using a mouse model carrying a mutant transgene encoding exon 1 of the human htt gene. Therefore, the application of our method is limited at present. However, even if wild-type htt is indeed essential for neuronal survival, it will certainly be possible to define an appropriate "therapeutic window" for partial suppression of the htt gene, thereby providing a new treatment strategy for HD.

References

Boado, R.J., Kazantsev, A., Apostol, B.L., Thompson, L.M., Pardridge, W.M., 2000. Antisense-mediated down-regulation of the human huntingtin gene. J. Pharmacol. Exp. Ther. 295, 239–243.

Bridge, A.J., Pebernard, S., Ducraux, A., Nicoulaz, A.L., Iggo, R., 2003. Induction of an interferon response by RNAi vectors in mammalian cells. Nat. Genet. 34, 263–264.

Busch, A., Engemann, S., Lurz, R., Okazawa, H., Lehrach, H., Wanker, E.E., 2003. Mutant huntingtin promotes the fibrillogenesis of wild-type huntingtin: a potential mechanism for loss of huntingtin function in Huntington's disease. J. Biol. Chem. 278, 41452–41461.

Chen, M., Ona, V.O., Li, M., Ferrante, R.J., Fink, K.B., Zhu, S., Bian, J., Guo, L., Farrell, L.A., Hersch, S.M., Hobbs, W., Vonsattel, J.P., Cha, J.H., Friedlander, R.M., 2000. Minocycline inhibits caspase-1 and caspase-3 expression and delays mortality in a transgenic mouse model of Huntington disease. Nat. Med. 6, 797–801.

DiFiglia, M., Sapp, E., Chase, K.O., Davies, S.W., Bates, G.P., Vonsattel, J.P., Aronin, N., 1997. Aggregation of huntingtin in neuronal intranuclear inclusions and dystrophic neurites in brain. Science 277, 1990–1993.

Dragatsis, I., Levine, M.S., Zeitlin, S., 2000. Inactivation of Hdh in the brain and testis results in progressive neurodegeneration and sterility in mice. Nat. Genet. 26, 300–306.

Duyao, M.P., Auerbach, A.B., Ryan, A., Persichetti, F., Barnes, G.T., McNeil, S.M., Ge, P., Vonsattel, J.P., Gusella, J.F., Joyner, A.L., 1995. Inactivation of the mouse Huntington's disease gene homolog Hdh. Science 269, 407–410.

Ferrante, R.J., Kubilus, J.K., Lee, J., Ryu, H., Beesen, A., Zucker, B., Smith, K., Kowall, N.W., Ratan, R.R., Luthi-Carter, R., Hersch, S.M., 2003. Histone deacetylase inhibition by sodium butyrate chemotherapy ameliorates the neurodegenerative phenotype in Huntington's disease mice. J. Neurosci. 23, 9418–9427.

Gines, S., Seong, I.S., Fossale, E., Ivanova, E., Trettel, F., Gusella, J.F., Wheeler, V.C., Persichetti, F., MacDonald, M.E., 2003. Specific progressive cAMP reduction implicates energy deficit in presymptomatic Huntington's disease knock-in mice. Hum. Mol. Genet. 12, 497–508.

Gusella, J.F., MacDonald, M.E., 2000. Molecular genetics: unmasking polyglutamine triggers in neurodegenerative disease. Nat. Rev. Neurosci. 1, 109–115.

Haque, N.S., Borghesani, P., Isacson, O., 1997. Therapeutic strategies for Huntington's disease based on a molecular understanding of the disorder. Mol. Med. Today 3, 175–183.

Harper, S.Q., Staber, P.D., He, X., Eliason, S.L., Martins, I.H., Mao, Q., Yang, L., Kotin, R.M., Paulson, H.L., Davidson, B.L., 2005. From the Cover: RNA interference improves motor and neuropathological abnormalities in a Huntington's disease mouse model. Proc. Natl. Acad. Sci. U.S.A. 102, 5820–5825.

Hazeki, N., Tsukamoto, T., Yazawa, I., Koyama, M., Hattori, S., Someki, I., Iwatsubo, T., Nakamura, K., Goto, J., Kanazawa, I., 2002. Ultrastructure

of nuclear aggregates formed by expressing an expanded polyglutamine. Biochem. Biophys. Res. Commun. 294, 429–440.

Kaytor, M.D., Wilkinson, K.D., Warren, S.T., 2004. Modulating huntingtin half-life alters polyglutamine-dependent aggregate formation and cell toxicity. J. Neurochem. 89, 962–973.

Kennedy, L., Evans, E., Chen, C.M., Craven, L., Detloff, P.J., Ennis, M., Shelbourne, P.F., 2003. Dramatic tissue-specific mutation length increases are an early molecular event in Huntington disease pathogenesis. Hum. Mol. Genet. 12, 3359–3367.

Liu, W., Goto, J., Wang, Y., Murata, M., Wada, K., Kanazawa, I., 2003. Specific inhibition of Huntington's disease gene expression by siRNAs in cultured cells. Proc. Jpn. Acad. 79 (Ser. B), 293–298.

Mangiarini, L., Sathasivam, K., Mahal, A., Mott, R., Seller, M., Bates, G.P., 1997. Instability of highly expanded CAG repeats in mice transgenic for the Huntington's disease mutation. Nat. Genet. 15, 197–200.

Mangiarini, L., Sathasivam, K., Seller, M., Cozens, B., Harper, A., Hetherington, C., Lawton, M., Trottier, Y., Lehrach, H., Davies, S.W., Bates, G.P., 1996. Exon 1 of the HD gene with an expanded CAG repeat is sufficient to cause a progressive neurological phenotype in transgenic mice. Cell 87, 493–506.

Menalled, L.B., Chesselet, M.F., 2002. Mouse models of Huntington's disease. Trends Pharmacol. Sci. 23, 32–39.

Nasir, J., Floresco, S.B., O'Kusky, J.R., Diewert, V.M., Richman, J.M., Zeisler, J., Borowski, A., Marth, J.D., Phillips, A.G., Hayden, M.R., 1995. Targeted disruption of the Huntington's disease gene results in embryonic lethality and behavioral and morphological changes in heterozygotes. Cell 81, 811–823.

Nellemann, C., Abell, K., Norremolle, A., Lokkegaard, T., Naver, B., Ropke, C., Rygaard, J., Sorensen, S.A., Hasholt, L., 2000. Inhibition of Huntington synthesis by antisense oligodeoxynucleotides. Mol. Cell Neurosci. 16, 313–323.

Novina, C.D., Murray, M.F., Dykxhoorn, D.M., Beresford, P.J., Riess, J., Lee, S.K., Collman, R.G., Lieberman, J., Shankar, P., Sharp, P.A., 2002. siRNA-directed inhibition of HIV-1 infection. Nat. Med. 8, 681–686.

Obrietan, K., Hoyt, K.R., 2004. CRE-mediated transcription is increased in Huntington's disease transgenic mice. J. Neurosci. 24, 791–796.

Sakurai, K., Iizuka, S., Shen, J.S., Meng, X.L., Mori, T., Umezawa, A., Ohashi, T., Eto, Y., 2004. Brain transplantation of genetically modified bone marrow stromal cells corrects CNS pathology and cognitive function in MPS VII mice. Gene Ther. 11, 1475–1481.

Schaffar, G., Breuer, P., Boteva, R., Behrends, C., Tzvetkov, N., Strippel, N., Sakahira, H., Siegers, K., Hayer-Hartl, M., Hartl, F.U., 2004. Cellular toxicity of polyglutamine expansion proteins: mechanism of transcription factor deactivation. Mol. Cell. 15, 95–105.

Shen, J.S., Meng, X.L., Ohashi, T., Eto, Y., 2002. Adenovirus-mediated prenatal gene transfer to murine central nervous system. Gene Ther. 9, 819–823.

Shen, J.S., Watabe, K., Ohashi, T., Eto, Y., 2001. Intraventricular administration of recombinant adenovirus to neonatal twitcher mouse leads to clinicopathological improvements. Gene Ther. 8, 1081–1087.

Song, E., Lee, S.K., Dykxhoorn, D.M., Novina, C., Zhang, D., Crawford, K., Cerny, J., Sharp, P.A., Lieberman, J., Manjunath, N., Shankar, P., 2003. Sustained small interfering RNA-mediated human immunodeficiency virus type 1 inhibition in primary macrophages. J. Virol. 77, 7174–7181.

Stephan, D.J., Yang, Z.Y., San, H., Simari, R.D., Wheeler, C.J., Felgner, P.L., Gordon, D., Nabel, G.J., Nabel, E.G., 1996. A new cationic liposome DNA complex enhances the efficiency of arterial gene transfer in vivo. Hum. Gene Ther. 7, 1803–1812.

Sugars, K.L., Brown, R., Cook, L.J., Swartz, J., Rubinsztein, D.C., 2004. Decreased cAMP response element-mediated transcription: an early event in exon 1 and full-length cell models of Huntington's disease that contributes to polyglutamine pathogenesis. J. Biol. Chem. 279, 4988–4999.

Tanaka, M., Machida, Y., Niu, S., Ikeda, T., Jana, N.R., Doi, H., Kurosawa, M., Nekooki, M., Nukina, N., 2004. Trehalose alleviates polyglutamine-mediated pathology in a mouse model of Huntington disease. Nat. Med. 10, 148–154.

Trushina, E., Heldebrant, M.P., Perez-Terzic, C.M., Bortolon, R., Kovtun, I.V., Badger 2nd, J.D., Terzic, A., Estevez, A., Windebank, A.J., Dyer, R.B., Yao, J., McMurray, C.T., 2003. Microtubule destabilization and nuclear entry are sequential steps leading to toxicity in Huntington's disease. Proc. Natl. Acad. Sci. U.S.A. 100, 12171–12176.

Tuschl, T., 2002. Expanding small RNA interference. Nat. Biotechnol. 20, 446–448.

Xia, H., Mao, Q., Eliason, S.L., Harper, S.Q., Martins, I.H., Orr, H.T., Paulson, H.L., Yang, L., Kotin, R.M., Davidson, B.L., 2004. RNAi suppresses polyglutamine-induced neurodegeneration in a model of spinocerebellar ataxia. Nat. Med. 10, 816–820.

Yamamoto, A., Lucas, J.J., Hen, R., 2000. Reversal of neuropathology and motor dysfunction in a conditional model of Huntington's disease. Cell 101, 57–66.

Yen, L., Strittmatter, S.M., Kalb, R.G., 1999. Sequence-specific cleavage of Huntingtin mRNA by catalytic DNA. Ann. Neurol. 46, 366–373.

Zeitlin, S., Liu, J.P., Chapman, D.L., Papaioannou, V.E., Efstratiadis, A., 1995. Increased apoptosis and early embryonic lethality in mice nullizygous for the Huntington's disease gene homologue. Nat. Genet. 11, 155–163.

Overexpression of Ubiquitin Carboxyl-Terminal Hydrolase L1 Arrests Spermatogenesis in Transgenic Mice

YU-LAI WANG,[1] WANZHAO LIU,[1] YING-JIE SUN,[2] JUNGKEE KWON,[1,3] RIEKO SETSUIE,[1,4]
HITOSHI OSAKA,[1] MAMI NODA,[4] SHUNSUKE AOKI,[1] YASUHIRO YOSHIKAWA,[3] AND KEIJI WADA[1]*

[1]Department of Degenerative Neurological Diseases, National Institute of Neuroscience, NCNP, Kodaira, Tokyo, Japan
[2]Department of Anatomy and Structural Science, Yamagata University School of Medicine, Yamagata, Japan
[3]Department of Biomedical Science, Graduate School of Agricultural and Life Sciences, University of Tokyo, Bunkyo-ku, Tokyo, Japan
[4]Laboratory of Pathophysiology, Graduate School of Pharmaceutical Sciences, Kyushu University, Higashi-ku, Fukuoka, Japan

ABSTRACT   Ubiquitin carboxyl-terminal hydrolase 1 (UCH-L1) can be detected in mouse testicular germ cells, mainly spermatogonia and somatic Sertoli cells, but its physiological role is unknown. We show that transgenic (Tg) mice overexpressing *EF1α* promoter-driven UCH-L1 in the testis are sterile due to a block during spermatogenesis at an early stage (pachytene) of meiosis. Interestingly, almost all spermatogonia and Sertoli cells expressing excess UCH-L1, but little PCNA (proliferating cell nuclear antigen), showed no morphological signs of apoptosis or TUNEL-positive staining. Rather, germ cell apoptosis was mainly detected in primary spermatocytes having weak or negative UCH-L1 expression but strong PCNA expression. These data suggest that overexpression of UCH-L1 affects spermatogenesis during meiosis and, in particular, induces apoptosis in primary spermatocytes. In addition to results of caspases-3 upregulation and Bcl-2 downregulation, excess UCH-L1 influenced the distribution of PCNA, suggesting a specific role for UCH-L1 in the processes of mitotic proliferation and differentiation of spermatogonial stem cells during spermatogenesis. *Mol. Reprod. Dev. 73: 40–49, 2006.* © 2005 Wiley-Liss, Inc.

Key Words: UCH-L1; transgenic mouse; spermatogenesis; testis; apoptosis

INTRODUCTION

Mammalian spermatogenesis is a complex process of cellular differentiation. Spermatogonia serve as the self-renewing stem cells for spermatogenesis and undergo mitotic divisions that yield primary spermatocytes (Matzuk and Lamb, 2002). In addition to germ cells, somatic Sertoli cells also are a major cell population in the testis, comprising the seminiferous tubule epithelium that nurtures germ cells (Imai et al., 2004).

Components of the ubiquitin system appear to be involved in different steps and processes during spermatogenesis (Baarends et al., 2000; Sutovsky, 2003).

© 2005 WILEY-LISS, INC.

Ubiquitin is a highly evolutionarily conserved 76-residue polypeptide that plays a critical role in many cellular processes, including the cell cycle, cell proliferation, development, apoptosis, signal transduction, and membrane protein internalization (Williams et al., 2002). Ubiquitin appears to be expressed in mammalian testes/ovaries and embryos at all developmental steps, and its level is modulated by ubiquitynating and deubiquitynating enzymes. However, the details of the involvement of these enzymes in ubiquitin-dependent proteolysis during gametogenesis and fertilization remain uncertain. Several deubiquitynating enzymes were recently reported (Wilkinson, 2000; Wing, 2003) and have been classified as either ubiquitin carboxyl-terminal hydrolases (UCHs) or ubiquitin-specific processing proteases. UCHs liberate free ubiquitin by cleaving ubiquitin-containing covalent complexes, namely ubiquitylated small ribosomal proteins (L40, S27a) or tandemly conjugated polyubiquitin (e.g., UbB, UbC) (Wilkinson, 2000). UCHs can also hydrolyze bonds between ubiquitin and small adducts or unfolded polypeptides in vitro. Thus, UCHs are thought to serve dual functions: to salvage ubiquitin that has been trapped by reactions with low-molecular weight thiols/amines and to process polyubiquitin or ubiquitylated proteins.

In mice, there are at least four closely related low-molecular weight UCH family members, UCH-L1 and UCH-L3–5 (Kurihara et al., 2001; Osawa et al., 2001). The distribution and function of UCH-L4 and UCH-L5 are not clear. UCH-L3, however, is expressed ubiquitously, whereas UCH-L1 is selectively expressed in the testis/ovary and brain. Moreover, UCH-L1 is highly

expressed in mouse spermatogonia and somatic Sertoli cells but not in post meiotic germ cells (Kwon et al., 2004a). By contrast, UCH-L3 is detected mainly in spermatocytes and round spermatids (Kwon et al., 2004a). These two isozymes are considered to play important roles in the labeling/targeting of abnormal proteins for degradation via the ubiquitin-proteasome system (Wilkinson, 2000).

The gracile axonal dystrophy (gad) mouse is an autosomal recessive spontaneous mutant carrying an intragenic deletion of the gene encoding UCH-L1 (Uchl1). gad mice do not express UCH-L1 and thus are comparable to a Uchl1 null mutant (Yamazaki et al., 1988; Saigoh et al., 1999). We recently showed that gad mice are resistant to the germ cell apoptosis during the first round of spermatogenesis (Kwon et al., 2005) and are also resistant to cryptorchid-induced testicular germ cell apoptosis (Kwon et al., 2004b). The expression of the apoptotic proteins p53, Bax, and caspases-3 was significantly lower in the immature testes, and the expression of both antiapoptotic and prosurvival proteins such as Bcl-2, Bcl-xL, XIAP, pCREB, and BDNF was significantly higher in gad mice following experimental cryptorchidism (Kwon et al., 2004b). These data prompted our hypothesis that UCH-L1 may be an important regulator of apoptosis during spermatogenesis. Experiments toward this end may provide additional evidence that UCH-L1 regulates spermatogenesis.

Our present report presents the characterization of the male sterility phenotype and the quantitation of apoptotic spermatocytes in Uchl1 transgenic (Tg) mice. Constitutive expression of UCH-L1 in the testis results in a blockade of spermatogenesis at the pachytene stage of spermatocytes due to an increase in the number of apoptotic spermatocytes. These results indicate that excess UCH-L1 affects spermatogenesis during meiosis and, in particular, induces apoptosis in primary spermatocytes.

MATERIALS AND METHODS
Animals

We have previously described the Tg Uchl1 mice carrying a 0.7-kb FLAG-tagged mouse Uchl1 cDNA with the human translation elongation factor-1α (EF-1α) promoter (Osaka et al., 2003). Tg mice were identified by PCR analysis of tail DNA using specific primers (forward: ex6F, 5'-ATCCAGGCGGCCCATGACCTC-3'; reverse: ex9R, 5'-AGCTGCTTTGCAGAGAGCCA-3'). The gad mouse is an autosomal recessive mutant that was obtained by crossing CBA and RFM mice (Saigoh et al., 1999). All strains were maintained at our institute. To corroborate fertility disturbances in UCH-L1 Tg mice, a subset of the mice was continuously mated with wild-type C57BL/6J mice. The mating of two heterozygous Tg males with non-Tg females did not yield offspring until the age of 6 months despite grossly normal appearance. This was also the case for the mating of four heterozygous Tg females with non-Tg males. Their non-Tg littermates sired offspring normally.

Finally, all six Tg mice were infertile, but they did not exhibit any apparent neurological phenotype during adulthood. Controls included nontransgenic (non-Tg) littermates and UCH-L1-deficient gad mice (Saigoh et al., 1999). Mice were sacrificed by cervical dislocation before tissue collection. Animal care and handling were in accordance with institutional regulations for animal care and were approved by the Animal Investigation Committee of the National Institute of Neuroscience, National Center of Neurology and Psychiatry of Japan.

mRNA Isolation, and Exogenous Uchl1 Expression Measured by Quantitative Real-Time RT-PCR

Total RNA from testes was isolated using the Trizol reagent (Gibco BRL Life Technologies, Bethesda, MD) and purified following the manufacturer's instructions. Real-time quantitative RT-PCR primer pairs flanking introns were used to specifically amplify transgene products, and their sequences were: forward, 5'-ATTT-CAGGTGTCGTGAGGAA-3'; and reverse, 5'-CCCAC-GTGGGAGACCTGATA-3'. Real-time quantitative PCR products, from 0.25–2.5 ng of reverse-transcribed cDNA samples, were detected using an ABI Prism, 7700 system (Applied Biosystems) as described previously (Aoki et al., 2002). β-Actin and GAPDH were used as endogenous controls. Results are expressed as the ratio of the mRNA level of the transgene to that of β-actin or GAPDH. As an external standard for quantitative analysis, the cDNA of the 3'-noncoding region of mouse Uchl1 cDNA (covering the RT-PCR primers) was cloned and inserted into a pcDNA3 vector, purified, precisely quantified, and serially diluted 10-fold to 10 copies/μl. Standard curves were determined using linear regression analysis of the Ct values relative to plasmid copy numbers. In each real-time quantitative PCR assay, a 10-fold serially diluted cDNA template series was added to construct a standard curve for copy number. Each sample was analyzed in triplicate, and copy numbers were determined from each corresponding standard curve by the ratio of Tg UCH-L1 to mouse Uchl1.

Histological Observations, Immunohistochemistry, and Immunofluorescence

Morphological studies were performed on six male controls and two male Tg mice (Tg21 and Tg22, both 6 months old). The two control groups consisted of three non-Tg wild-type C57BL/6J mice, 6 months old, littermates, and three gad mice, age 4 months. Testes were fixed in 4% paraformaldehyde for 24 hr and embedded in paraffin. Serial 5-μm sections were used for histology after hematoxylin–eosin staining as well as for immunohistochemistry and the TUNEL assay. Primary monoclonal or polyclonal antibodies against the following proteins were used at the final dilutions indicated: UCH-L1 (RA95101, Ultraclone, Lucigen, Middleton, WI, 1:2,000), FLAG (FM2, Sigma, St. Louis, MO, 1:500), PCNA (PC10, Santa Cruz Biotechnology, Santa Cruz, CA, 1:200), PCNA (Clone 24, BD Transduction

Laboratory, Lexington, KY, 1:2,000), vimentin (Zymed, 1:100), and ubiquitin (Dako, Carpenteria, CA, 1:400). For controls, the primary antibody was replaced with normal rabbit serum or was omitted (these controls always yielded negative staining). For immunofluorescence studies, secondary antibodies were anti-mouse-Cy3 or -FITC or anti-rabbit-conjugated-Cy3 or -FITC (Jackson ImmunoResearch, West Grove, PA, 1:500).

TUNEL Assay

TUNEL staining was performed according to the original protocol, with modifications (Harada et al., 2004). The number of apoptotic cells was determined by counting positively stained nuclei in 30 tubule cross-sections per testis section in each testis (Kwon et al., 2004b). For clarity and brevity, we also counted all the TUNEL-stained cells within the entire cell population of testicular tubules in each section. In addition, we also counted the apoptosis-positive tubules (i.e., tubules containing at least one apoptotic cell) in each testis.

Western Blotting

Protein lysates were prepared from mouse testes as described (Kwon et al., 2004b). Approximately 20 μg of total protein was loaded per lane on 15% SDS–PAGE gels. Primary antibodies (diluted as indicated) were used to detect the following proteins: UCH-L1 (RA95101, 1:5,000), FLAG (FM2, Sigma, 1:2,000), Bcl-2 (Cell Signaling, Beverly, MA, 1:1,000), caspase-3 (Cell Signaling, 1:400), polyubiquitin (FK2 clone, Medical & Biological Laboratory, Nagoya, Japan, 1:1,000), and monoubiquitin (U5379, Sigma, 1:1,000). Blots were further incubated with peroxidase-conjugated goat anti-mouse IgG or goat anti-rabbit IgG (1:5,000; Pierce, Rockford, IL) for 1 hr at room temperature. Immunoreactions were visualized using the SuperSignal West Dura extended duration substrate (Pierce) and analyzed with a ChemiImager (Alpha Innotech, San Leandro, CA). ChemiImager data were analyzed using AlphaEase software (Alpha Innotech) to yield the relative level of each protein.

RESULTS

Sterile Phenotype of *Uchl1* Tg Mice

We initially attempted to overexpress *Uchl1* in neurons using a Tg construct containing the *EF-1α* promoter (Mizushima and Nagata, 1990). The transgene was also strongly expressed in gonads as well as other Tg mice via the same promoter (Furuchi et al., 1996). We obtained six Tg mice having high transgene copy number, each of which most likely carried the transgene in a unique genomic location (see below). Four of these mice were females (Tg11, Tg12, Tg43, Tg81) and two were males (Tg21 and Tg22). Unexpectedly, all of these Tgs were sterile. Thus, it was not possible to maintain Tg lines during the course of these experiments. However, in addition to the sterile phenotype, the six independent Tg mice showed a similar pattern of *Uchl1* transgene expression and common pathological defects, the latter being limited to the testes or ovaries.

The Tg loci were generated by random integration rather than by site-specific recombination, and thus the animals produced by our Tg procedure usually had more than one transgene integrated at each chromosomal site (Kroll and Amaya, 1996). Therefore, in each of the six Tg mice, the transgene most likely integrated into a different genomic site, raising the possibility of different position-dependent effects. Our data showed that we obtained multiple animals with similar patterns or levels of *Uchl1* transgene expression and with common pathological defects, suggesting the phenotypes reflect position-independent expression (i.e., independent of the position of transgene insertion). Thus, these Tg mice had similar infertile phenotypes that may be attributed to the overproduction of UCH-L1. Numerous gene inactivation studies have identified gene products involved in male fertility, but in most cases female reproduction was unaffected or weak damaged (Yuan et al., 2000). However, both male and female *Uchl1* Tg mice were infertile, although there were clear differences in germinal cell maturation, suggesting that UCH-L1 is required for both spermatogenesis and oogenesis. Therefore, six independent Tg founders, notably two males (Tg21 and Tg22), were analyzed in our present study.

The mating of two heterozygous Tg males with non-Tg females did not yield offspring until the age of 6 months, despite grossly normal appearance. This was also the case for the mating of four heterozygous Tg females with non-Tg males. Their non-Tg littermates sired offspring normally. At autopsy, the testes of both Tg21 and Tg22 appeared grossly smaller than those of non-Tg mice. The testes weight of Tg21 (77 mg) and Tg22 (70 mg) was only 42% and 38%, respectively, relative to non-Tg males (183 ± 16 mg), demonstrating that mice overexpressing UCH-L1 display profoundly defective testis development.

Expression Levels of the *Uchl1* Transgene

We used RT-PCR and primers specific for the *Uchl1* transgene to compare transgene expression levels in the testes or ovaries of the six Tg mice. There was some variation between animals (Fig. 1A). All the Tgs expressed a similar level of endogenous *Uchl1* mRNA (Fig. 1A); quantitation of absolute Tg *Uchl1* copy numbers using real-time quantitative RT-PCR showed that all six Tgs expressed 2.9–6.8-fold more *Uchl1* transgene mRNA compared with endogenous mRNA (4.5, 3.6, 6.2, 3.7, 2.9, and 6.8 for Tg21, Tg22, Tg11, Tg12, Tg43, and Tg81, respectively). Relative UCH-L1 protein expression was similar among four of the Tgs (76.1 ± 5.2; Fig. 1B) but was somewhat higher in Tg 21 (100) and Tg81 (106.2). The average level of endogenous UCH-L1 expression in Tg mice was ~91% relative to non-Tg mice (Fig. 1B).

Immunohistochemistry of testicular sections using an antibody against FLAG revealed that exogenous UCH-L1 localized mainly in spermatogonia and Sertoli cells (Fig. 2E), similar to the localization of endogenous UCH-L1 (Fig. 2A). Endogenous UCH-L1 localized to both the cytoplasm and nucleus of spermatogonia and Sertoli
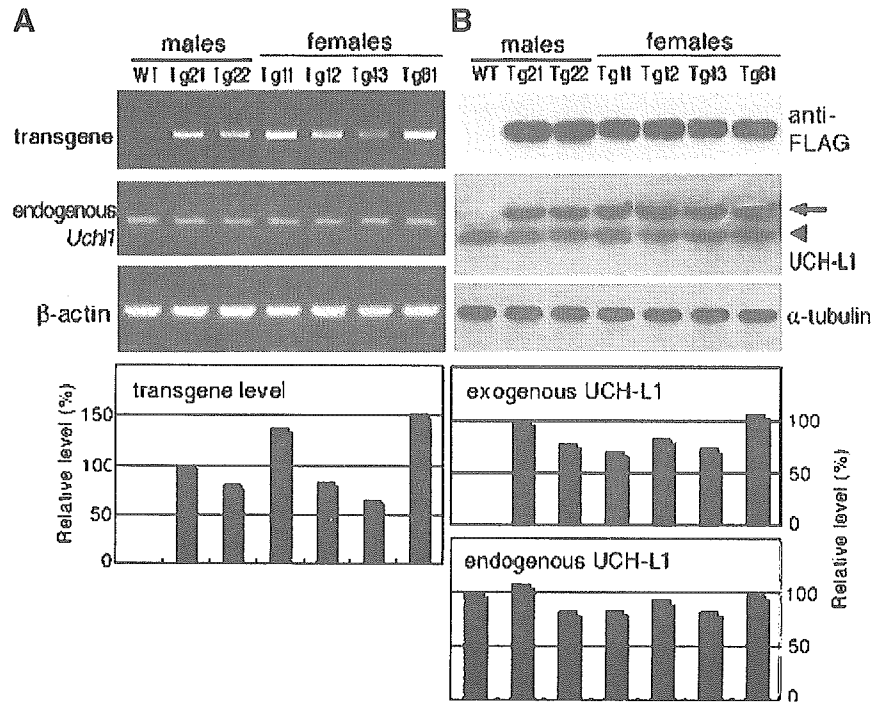
Fig. 1. Expression of transgenic ubiquitin carboxyl-terminal hydrolase 1 (UCH-L1) in the testes of Tg21 and Tg22 male mice. **A:** Transgenic *Uchl1* mRNA levels in the testes. RT-PCR showed high levels of *Uchl1* transgene mRNA in both Tg21 and Tg22 as well as in all ovaries from four female Tg mice. All Tg mice had a normal level of endogenous *Uchl1* mRNA. The relative expression level is indicated below each lane (as a percentage, scaled to β-actin in each lane). **B:** Western blot analysis of testicular or ovarian lysates. Both endogenous and exogenous UCH-L1 were detected with anti-UCH-L1, whereas exogenous UCH-L1 was specifically detected by anti-FLAG. Exogenous UCH-L1 (arrow) is slightly larger than endogenous UCH-L1 (arrowhead). WT, non-Tg wild-type.
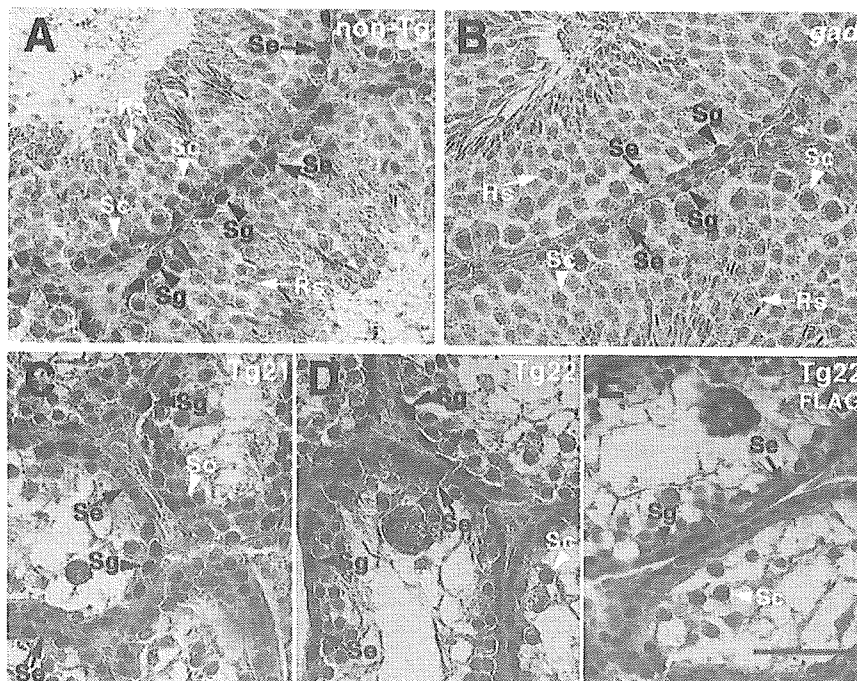

Fig. 2. Immunostaining of FLAG and UCH-L1 in *Uchl1* Tg mice shows high levels of UCH-L1 in testicular tubules. UCH-L1 immunostaining is clearly present in spermatogonia (Sg) and Sertoli cells (Se) of a non-Tg mouse (**A**) but not in a *gad* mouse (**B**). In contrast, in the testes of two Tg males, the most intense UCH-L1 immunoreactivity occurs predominantly in spermatogonia (Sg, arrowheads) and Sertoli cells (Se, arrows) but not in the primary spermatocytes (Sc, white arrowheads; **C**, Tg21; **D**, Tg22). **E:** Immunostaining of FLAG confirmed the transgene-derived UCH-L1 proteins in spermatogonia (Sg, arrowheads) and Sertoli cells (Se, arrows) but not in the primary spermatocytes (Sc, white arrowheads; Tg22). Magnification: ×400. Scale bar, 50 μm.

cells in the testes of non-Tg males; however, localization was not apparent around pachytene spermatocytes or round, elongated spermatids (Fig. 2A). This distribution of UCH-L1 is in good agreement with previous reports (Kon et al., 1999; Kwon et al., 2004a). Compared with non-Tg males, overexpression of UCH-L1 in seminiferous tubules of Tg males (Tg21 and Tg22) occurred predominantly in spermatogonia and Sertoli cells, and was weakly positive or negative in spermatocytes (Fig. 2C,D). These data coincided with strong induction of the *Uchl1* transgene. Tg mice expressed a higher level of total UCH-L1 (both endogenous and exogenous), suggesting a correlation between excess UCH-L1 and sterility.

Morphological Examination

Histopathological analysis of testes from 6-month-old Tg21 and Tg22 revealed terminal loss of differentiated germ cells and a large number of pachytene spermatocytes that had degenerated (with condensed nuclei and giant cells) and been sloughed off, forcing an altered structure of the seminiferous tubules such that they appeared almost empty (Fig. 3A). The deformed seminiferous tubules also contained numerous arrested spermatocytes (Fig. 3A, arrowheads) and multinucleated giant cells (arrows). In contrast, the seminiferous tubules of *gad* mice were nearly intact, as in non-Tg males (data not shown). In non-Tg males, seminiferous tubules containing elongated spermatids in the inner layer were readily detected (data not shown), whereas these tubules were scarcely detectable in Tg21 (Fig. 3A) and Tg22. On the other hand, the four female Tg mice displayed a variety of phenotypes, including an increased number of apoptotic oocytes and granulosa cells relative to non-Tg females, leading to infertility (data not shown).

In non-Tg (Fig. 3B) and *gad* mice (Fig. 3C), only a few TUNEL-positive cells were identified, located at the periphery of the tubule. However, many fewer TUNEL-positive cells were detected in the Tg males (Fig. 3D,E), and cell morphology indicated that most of these positive cells were primary spermatocytes. However, neither the TUNEL assay nor microscopy revealed evidence of apoptosis in spermatogonia or Sertoli cells. We quantitatively assessed germ cell apoptosis in Tg, non-Tg, and *gad* mice by calculating the number of apoptotic cells per tubules in each testis. This value was 25 times higher in Tg testes compared with non-Tg or *gad* testes (the averages $\pm$ SD were as follows: 553 ± 72, n = 2 in Tg testes; 22 ± 4.2, n = 3 in non-Tg; and 21 ± 5.3, n = 3 in *gad*). The percentage of apoptosis-positive tubules in Tg testes was also significantly higher than in non-Tg or *gad* mice (the averages $\pm$ SD were as follows: 95.3 ± 2.7, n = 2 in Tg testes; 7.4 ± 2.2, n = 3 in non-Tg; and 7.1 ± 1.8, n = 3 in *gad*).

A control section of caput epididymis, an androgen-dependent organ, from same Tg mice was investigated. No UCH-L1 overexpressing was detected, and no pathological symptoms could be observed in the epididymis (data not shown).
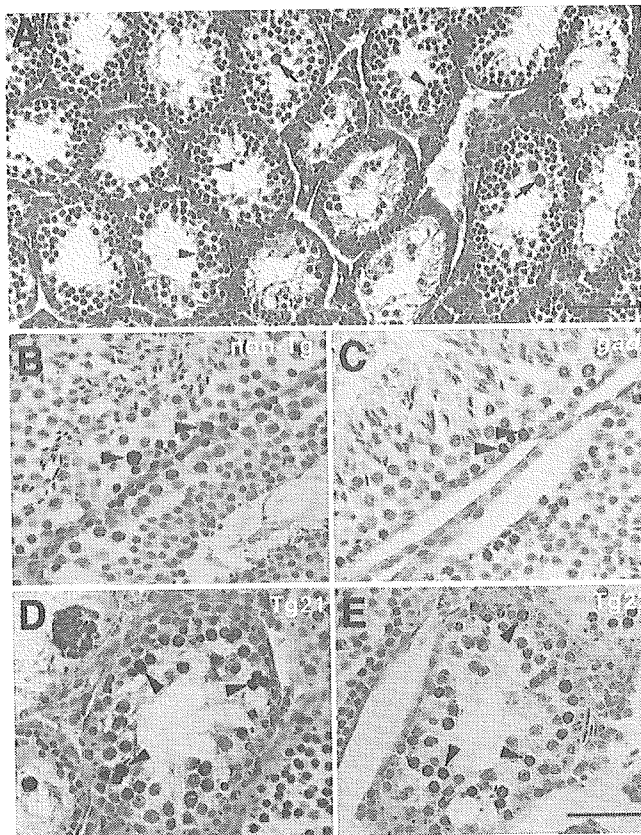

Fig. 3. Histopathology and TUNEL assay in situ. A: Hematoxylin–eosin staining of testis sections from the Tg21 male mouse shows defective spermatogenesis. Arrowheads indicate arrested spermatocytes and arrows indicate giant cells. Round spermatocytes and spermatids were rarely observed. B–E: Examples of TUNEL-positive cells characterized by the robust deposition of the reddish brown reaction product in sections of testis from non-Tg (B), *gad* (C), and Tg mice (D, Tg21; E, Tg22). Sections were counterstained with hematoxylin. A large number of TUNEL-positive cells were clearly observed at the periphery of the seminiferous tubule (arrowheads) in Tg21 (D) and Tg22 (E), whereas a lesser number of positives were apparent in non-Tg (B) or *gad* mice (C). Most of these positive cells appeared to be primary spermatocytes. Magnification: (A) ×100; (B–E) ×400. Scale bar in (A) 200 μm; (E) 50 μm.

UCH-L1 Relates to the Expression of PCNA

PCNA expression is associated with cell proliferation and DNA synthesis during S phase of the cell cycle and DNA repair in non-dividing cells (Kelman, 1997; Toschi and Bravo, 1988). Unlike UCH-L1, which is abundant in brain, PCNA is not detectable in the central nervous system (Saigoh et al., 1999; Williams et al., 2002). In the testis, PCNA is expressed in germ cells and Sertoli cells, and the nuclear localization of PCNA overlaps with that of UCH-L1 in monkey testis (Tokunaga et al., 1999). Our recent study showed that mice lacking UCH-L1 have significantly decreased numbers of PCNA-positive cells in seminiferous tubules (Kwon et al., 2003). These results led us to hypothesize that UCH-L1 may be closely associated with spermatogonial proliferation activity, possibly to maintain the primordial nature of these cells. We thus immunostained testes for PCNA

and UCH-L1. In non-Tg and *gad* testes, PCNA-positive staining was confined to spermatogonia and primary spermatocytes and was not evident in Sertoli cells (Fig. 4A,D,B,E) Similarly, the percentage of PCNA-positive spermatogonia and spermatocytes in the seminiferous tubules of *gad* mice was significantly lower than that of non-Tg mice (Fig. 4A,D,B,E) as we previously observed (Kwon et al., 2003). In contrast, Tg mouse testes showed greater PCNA staining in these cells; surprisingly however, staining was observed in nearly all arrested primary spermatocytes but not in spermatogonia (Fig. 4F). These findings suggest that

UCH-L1 plays a specific role in mitotic proliferation. To further clarify the effect of UCH-L1 on PCNA levels, FLAG-tagged *Uchl1* was transfected into GC-1, a germ cell line derived from type B spermatogonia (Hofmann et al., 1992). UCH-L1 (anti-FLAG, Fig. 4G,I, green) and PCNA (Fig. 4H,I, red) were then visualized using immunofluorescence microscopy. Cells transfected with *Uchl1* showed lower PCNA immunoreactivity compared with mock-transfected cells (Fig. 4G), consistent with the assertion that PCNA is downregulated by UCH-L1 in vivo. However, no change of PCNA level was observed in *Uchl3* transfected cells (data not shown),
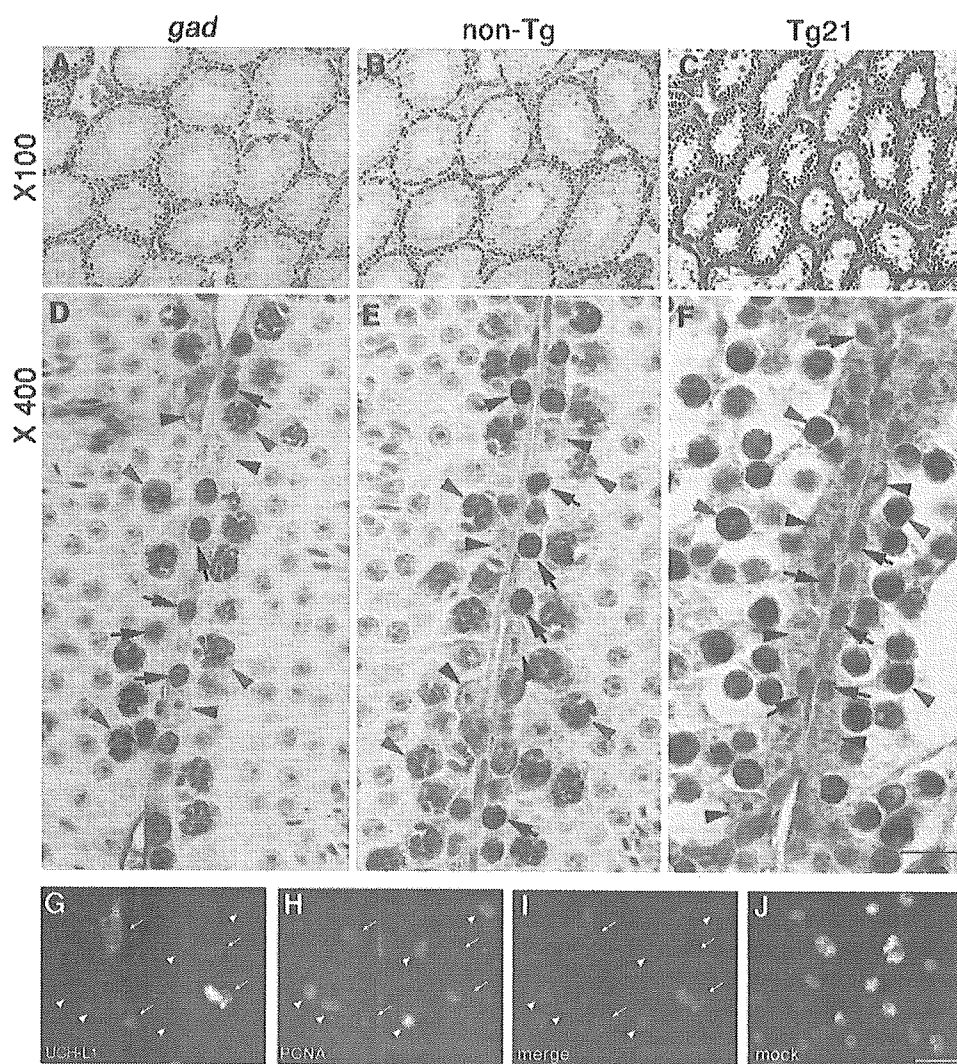

Fig. 4. PCNA immunostaining in the testes of a *gad* mouse (A, D), a non-Tg mouse (B, E), a Tg mouse (C, F; Tg21), and in the transient transfection assay with UCH-L1 using GC-1 cells (G–J). In *gad* and non-Tg testes, positive immunostaining was confined to spermatogonia (D, E; black arrows) and primary spermatocytes (D, E; red arrowheads), and staining was not seen in Sertoli cells (D, E; black arrowheads). In contrast, cell staining was more intense in the testis of Tg mice; however, this intensity was observed in almost all arrested primary spermatocytes (F; red arrowheads) but not in spermatogonia (F; black arrows). The staining of non-Tg and *gad* mice was essentially identical. However, nearly all the primary spermatocytes from Tg mice had relatively strong reactivity compared with spermatogonia that had

very faint PCNA reactivity (black arrows). Plasmid pCIneo-*Uchl1* (G–I) or vector alone (J, mock) was transfected into GC-1 cells and expressed. Antibodies against FLAG (Sigma, monoclonal) and PCNA (BD Transduction Laboratory, polyclonal) were used to detect exogenously expressed UCH-L1 (G, I, green) and endogenous PCNA (H, J, I, red), respectively. Cells expressing a high level of UCH-L1 (G, white arrows) had a relative low level of PCNA (H, white arrows), whereas cells expressing a low level of UCH-L1 (H, white arrowheads) had high PCNA levels (H, white arrowheads). Magnification: (A–C) ×100; (D–J) ×400. Scale bar: **Upper panels** (see **panel C**), 200 µm; **middle panels** (see **panel F**), 50 µm; **lower panels** (see **panel J**), 50 µm.
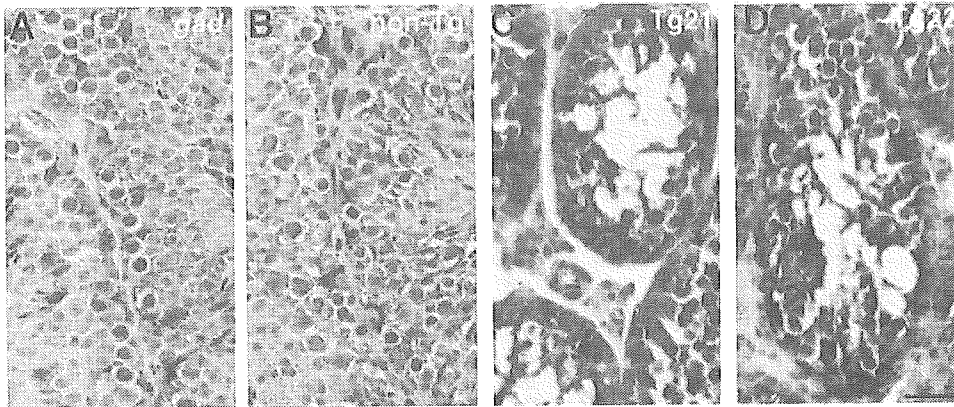
Fig. 5. Vimentin immunostaining in the testes of a *gad* mouse (**A**), a non-Tg mouse (**B**), and Tg mice (**C**, Tg21; **D**, Tg22). No difference was observed in the pattern and density of vimentin staining in Sertoli cells between *gad* (A) and non-Tg testes (B). In contrast, Sertoli cell staining was more intense in the Tg mice (C, D). Magnification: ×400. Scale bar, 200 μm.

suggesting the specificity of UCH-L1 effect on PCNA levels.

Sertoli Cells Exhibit High-Level Vimentin Expression in Tg Mice

We examined the immunoreactivity to vimentin, which is a marker of Sertoli cells (Oke and Suarez-Quian, 1993; Mori et al., 1997). Vimentin immunostaining was observed in Sertoli cells, and there is no difference between *gad* and non-Tg mice (Fig. 5A,B). In contrast, véry strong expression of vimentin was observed in almost all Sertoli cells throughout the cytoplasm in Tg mice (Fig. 5C,D).

Bcl-2 Downregulation and Caspase-3 Upregulation in Tg Mice

The two key proteins, Bcl-2 and caspases-3 that involved in testicular germ cell apoptosis are especially altered during spermatogenesis or stress-induced germ cell apoptosis in *gad* mice (Harada et al., 2004; Kwon et al., 2004b, 2005). We thus examined the expression of these proteins in Tg and non-Tg testes to determine whether they are actually involved in countering increased apoptosis. Bcl-2 expression was downregulated in the testes of Tg mice compared with non-Tg mice (Fig. 6). In contrast to non-Tg mice, Tg mice had an elevated level of the activated caspase-3 subunit, p17 (Fig. 6), controversial to that observed in the retina of *gad* mice after ischemic injury (Harada et al., 2004). These results are consistent with the profound difference in UCH-L1 expression in these two mouse lines.

Upregulations of both Mono- and Poly-Ubiquitin in Tg Mice

Our recent studies suggested novel functions for UCH-L1, namely that it effectively upregulates ubiquitin levels at the post-transcriptional level (Osaka et al., 2003) and that ubiquitin induction plays a critical role in regulating cell death during cryptorchid injury—mediated germ cell apoptosis (Kwon et al., 2004b). Moreover, the testes of mice expressing K48R

mutant ubiquitin are protected from cryptorchid injury (Rasoulpour et al., 2003). Given this information, we examined ubiquitin levels in *Uchl1* Tg mice. As expected, ubiquitin expression was strong in testicular cells of Tg mice (Fig. 7C,D), particularly in the arrested spermatocytes, but its expression was low in *gad* mice (Fig. 7B) compared with non-Tg mice (Fig. 7A). These data provide additional evidence that ubiquitin expression is induced upon UCH-L1 overexpression. To determine whether the increased ubiquitin staining represented monoubiquitin or polyubiquitin, we next examined the levels of both ubiquitin forms via immunoblotting (Fig. 7E). As expected, mono- and poly-ubiquitin levels in Tg mice were substantially higher than in non-Tg mice. A *gad* mouse control had relatively low levels
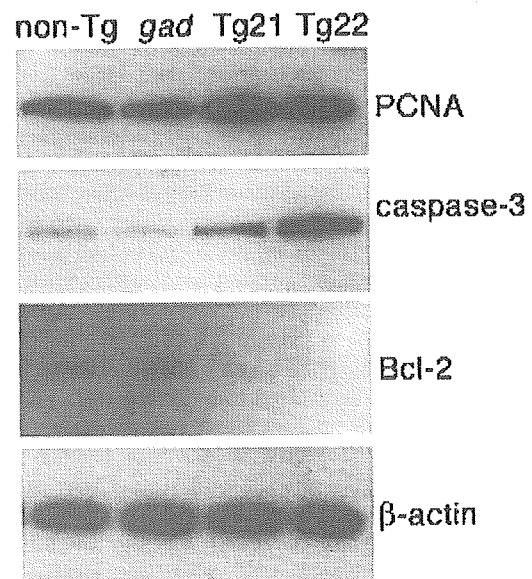

Fig. 6. Western blot analysis of Tg mouse testicular lysates. Consistent with the immunohistochemistry results, PCNA and caspase-3 substantially accumulated in Tg mice. However, the expression of antiapoptotic Bcl-2 decreased compared with non-Tg or *gad* mice.
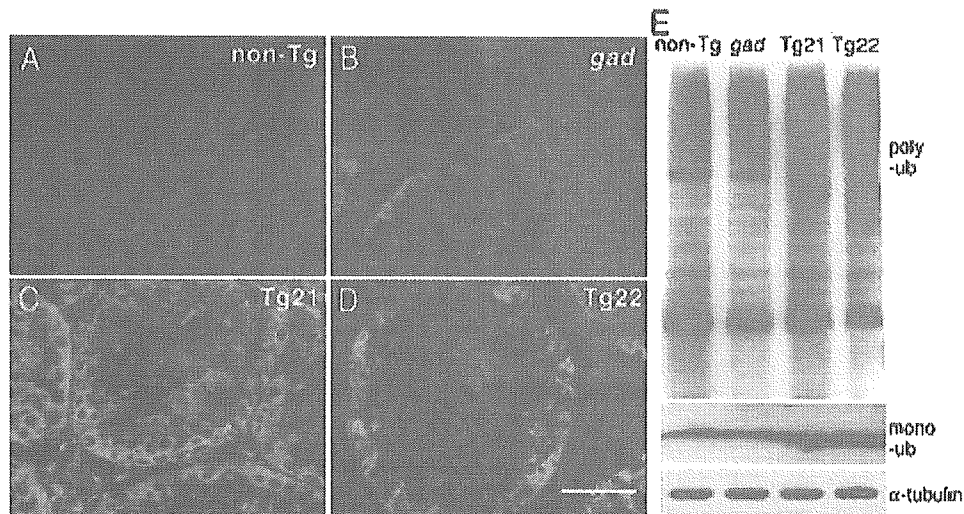
Fig. 7. The levels of mono- and poly-ubiquitin in the testes of non-Tg and Tg males. Double immunostaining for UCH-L1 and ubiquitin in the testis (A, non-Tg; B, *gad*; C, Tg21; D, Tg22). All strongly UCH-L1-positive cells (green) were also strongly positive for ubiquitin (red) in the two male Tg mice. Scale bar, 50 μm. E. An immunoblot showing that both mono- and poly-ubiquitin expression were significantly increased in the two Tg mice compared with non-Tg and *gad* mice (ub, ubiquitin).

of both mono- and poly-ubiquitin (Fig. 7E). These findings are consistent with previous studies and support the hypothesis that UCH-L1-mediated spermatocyte apoptosis involves the induction of ubiquitin expression.

DISCUSSION

Apoptosis in testicular germ cells is regulated by a complicated signal transduction pathway; however, the molecular mechanisms regulating this process are uncertain. We recently showed that *gad* mice, lacking UCH-L1 function, are resistant to apoptotic stress (Harada et al., 2004; Kwon et al., 2004b). These observations conclusively indicate that UCH-L1 plays a role in germ cell death during experimental stress-induced apoptosis. We thus hypothesized that germ cell apoptosis is directly induced by excess UCH-L1. To test this hypothesis, we utilized three mouse lines, wild-type (non-Tg), *gad* and *Uchl1* Tgs, which differ with respect to UCH-L1 expression. In Tg mice, germ cell apoptosis was barely detectable in spermatogonia or Sertoli cells, both of which strongly expressed UCH-L1. Apoptosis was observed mainly in primary spermatocytes, which had weak or negative UCH-L1 expression although they are derived from spermatogonia. These data suggest that excess UCH-L1 in fact does not directly induce apoptosis in spermatogonia or somatic Sertoli cells. These data further provoke the question of why apoptosis occurs during spermatocyte meiosis.

In our *Uchl1* Tg mice, there was no evidence of spermatogonia or Sertoli cell apoptosis despite the fact that these cells had stronger UCH-L1 expression compared with non-Tg mice. Accordingly, it could be concluded that overexpression of UCH-L1 in spermatogonia does not directly induce apoptosis in these cells (nor in Sertoli cells). Because spermatocytes are geneti-

cally distinct from the original mother cell (spermatogonia), we speculate that the Tg mice are highly susceptible to spermatocyte apoptosis in vivo, with the inference that spermatocytes seem to be particularly sensitive to UCH-L1 overexpression in spermatogonia even though spermatocytes themselves express a much lower level of UCH-L1. In contrast, *gad* mice are resistant to cryptorchid-induced germ cell apoptosis, and many germ cells undergo apoptosis in older animals although their testes develop nearly normally and produce mature sperm (Kwon et al., 2004b). These data suggest that the lack of UCH-L1 causes mice to have lower sensitivity to stress compared with wild-type males, although UCH-L1 is probably not essential for spermatogenesis under normal conditions. On one hand, UCH-L1 seems to be necessary for the stabilization of germ cells to protect against aging-associated apoptosis; however, the stabilization of germ cells appears to be limited by the concentration of UCH-L1, and consequently they may be damaged during spermatocyte meiosis when UCH-L1 is overexpressed. Despite the fact that excess UCH-L1 does not induce spermatogonial apoptosis, abnormalities in intracellular regulatory factors may potentially influence mitosis directly (i.e., as the cell divides into two daughter cells—spermatocytes). Some of these factors may accumulate or be reduced in the presence of excess UCH-L1, thereby causing disruptions such as arrested meiosis or the onset of apoptosis in spermatocytes rather than spermatogonia (Fig. 8).

Many of the factors involved in cellular apoptosis, including the Bcl-2 family and caspases, are targets for ubiquitynation. Previously, we have shown that Bcl-2 is upregulated (Kwon et al., 2004b) and caspases-3 is downregulated (Kwon et al., 2005) in *gad* mice. The decreased level of Bcl-2 and increased level of caspases-3